BRIGHAM YOUNG UNIVERSITY

GEOLOGY

STUDIES

GEOLOGICAL SOCIETY OF AMERICA

FIELD TRIP GUIDE BOOK

1997 ANNUAL MEETING • SALT LAKE CITY, UTAH

PART 2 TWO

EDITED BY PAUL KARL LINK AND BART J. KOWALLIS

VOLUME 42 • 1997

MESOZOIC TO RECENT GEOLOGY OF UTAH

Edited by
Paul Karl Link and Bart J. Kowallis

BRIGHAM YOUNG UNIVERSITY GEOLOGY STUDIES

Volume 42, Part II, 1997

CONTENTS

A Publication of the
Department of Geology
Brigham Young University
Provo, Utah 84602

Brigham Young University Geology Studies is published by the Department of Geology. This publication consists of graduate student and faculty research within the department as well as papers submitted by outside contributors. Each article submitted is externally reviewed by at least two qualified persons.

Cover photos taken by Paul Karl Link.

Top: Upheaval Dome, southeastern Utah.
Middle: Lake Bonneville shorelines west of Brigham City, Utah.
Bottom: Bryce Canyon National Park, Utah.

ISSN 0068-1016
9-97 700 23870/24290

Preface

Guidebooks have been part of the exploration of the American West since Oregon Trail days. Geologic guidebooks with maps and photographs are an especially graphic tool for school teachers, University classes, and visiting geologists to become familiar with the territory, the geologic issues and the available references.

It was in this spirit that we set out to compile this two-volume set of field trip descriptions for the Annual Meeting of the Geological Society of America in Salt Lake City in October 1997. We were seeking to produce a quality product, with fully peer-reviewed papers, and user-friendly field trip logs. We found we were bucking a tide in our profession which de-emphasizes guidebooks and paper products. If this tide continues we wish to be on record as producing "The Last Best Geologic Guidebook."

We thank all the authors who met our strict deadlines and contributed this outstanding set of papers. We hope this work will stand for years to come as a lasting introduction to the complex geology of the Colorado Plateau, Basin and Range, Wasatch Front, and Snake River Plain in the vicinity of Salt Lake City. Index maps to the field trips contained in each volume are on the back covers.

Part 1 "Proterozoic to Recent Stratigraphy, Tectonics and Volcanology: Utah, Nevada, Southern Idaho and Central Mexico" contains a number of papers of exceptional interest for their geologic synthesis. Part 2 "Mesozoic to Recent Geology of Utah" concentrates on the Colorado Plateau and the Wasatch Front.

Paul Link read all the papers and coordinated the review process. Bart Kowallis copy edited the manuscripts and coordinated the publication via Brigham Young University Geology Studies. We would like to thank all the reviewers, who were generally prompt and helpful in meeting our tight schedule. These included: Lee Allison, Genevieve Atwood, Gary Axen, Jim Beget, Myron Best, David Bice, Phyllis Camilleri, Marjorie Chan, Nick Christie-Blick, Gary Christenson, Dan Chure, Mary Droser, Ernie Duebendorfer, Tony Ekdale, Todd Ehlers, Ben Everitt, Geoff Freethey, Hugh Hurlow, Jim Garrison, Denny Geist, Jeff Geslin, Ron Greeley, Gus Gustason, Bill Hackett, Kimm Harty, Grant Heiken, Lehi Hintze, Peter Huntoon, Peter Isaacson, Jeff Keaton, Keith Ketner, Guy King, Mel Kuntz, Tim Lawton, Spencer Lucas, Lon McCarley, Meghan Miller, Gautam Mitra, Kathy Nichols, Robert Q. Oaks, Susan Olig, Jack Oviatt, Bill Perry, Andy Pulham, Dick Robison, Rube Ross, Rich Schweickert, Peter Sheehan, Norm Silberling, Dick Smith, Barry Solomon, K.O. Stanley, Kevin Stewart, Wanda Taylor, Glenn Thackray and Adolph Yonkee. In addition, we wish to thank all the dedicated workers at Brigham Young University Print Services and in the Department of Geology who contributed many long hours of work to these volumes.

Paul Karl Link and Bart J. Kowallis, Editors

Quaternary Geology and Geomorphology, Northern Henry Mountains Region

BENJAMIN L. EVERITT
Utah Division of Water Resources, 1594 W. North Temple, Salt Lake City, Utah 84114-6201

ANDREW E. GODFREY
USDA Forest Service, Intermountain Region, 324 25th St., Ogden, Utah 84401

ROBERT S. ANDERSON
Department of Earth Sciences, University of California, Santa Cruz, California 95064

ALAN D. HOWARD
Department of Environmental Sciences, University of Virginia, Charlottesville, Virginia 22903

PART 1—ROAD LOG

Ben Everitt and Andrew E. Godfrey

The following road log describes the Fremont River and the northern piedmont of the Henry Mountains. The field trip is designed to bring together summaries of current research from a variety of sources and place them in a historical and geologic context. Two broad subject areas of the geomorphology of the northern Henry Mountains region are presented in the road log and associated papers. One subject covers the history of the gravel deposits along the Fremont River and northward from Mount Ellen. The second includes some of the erosion processes of the Mancos Shale in the Upper Blue Hills Badlands.

Three papers describe erosion processes on the Mancos Shale. Dick, et.al., hypothesize that network geometry of small drainages exerts a significant control on a hydrograph's shape when flow is produced by high-intensity storms that are short relative to the rise time of the hydrograph. This is because tributary flows are short-lived and contribute to the trunk channel peaks that are preserved in the outflow hydrograph. For similar-sized but longer-duration storms they found that the hydrograph rises slowly, with smaller peaks that are not clearly preserved in the outflow hydrograph. Godfrey's paper on wind erosion showed that sudden gusts in southwest winds can produce short-lived pressure drops on the lee sides of southeast-trending ridges. The resulting pressure difference between the soil atmosphere and the air above can lift the surface crust to be blown away. Resulting landforms include hollows and notches near the top of the ridges, and northeast facing cliffs, some with shallow, closed depressions in front. Godfrey's 30-year study of soil creep showed an average rate of 2.7 cm/yr on slopes averaging 35 degrees. Slope aspect did not appear to affect rates, but the upper meter or two moved at a significantly slower rate than lower portions of a slope. Winters with two or more consecutive days of at least 6 mm precipitation showed episodes of accelerated creep or shallow slumping.

Two paper discuss gravel deposits. Repka, et.al., dated terraces along the Fremont River using cosmogenic methods. They found age estimates of 60, 102, and 151 ka for the three most extensive terraces. This led then to the conclusion that the terraces were formed when there was a strong glacial source in the headwaters, and were abandoned when the sediment source shut off. In contrast, Godfrey's mapping of shoestring gravel deposits between Mount Ellen and the Fremont River suggests that random stream captures, rather than climate fluctuations, produced the various bench levels.

Everitt's observations, contained in the road log, show that alluvial fill in the Fremont-Dirty Devil river valley thins downstream from 80 feet below river level near Torrey, to 50 feet near Caineville, then thickens again to more than 100 feet at Hanksville. The thick alluvial fills, terraces, and buried canyons of the Fremont River system contain a record of the complex response of the river to the waxing and waning of Pleistocene glaciers in its headwaters, the changing precipitation regimes in its arid lower reaches, and the inconstant base level of the Colorado River to which it is tributary.

Observations by Everitt of the vegetation along the Fremont River flood plain show that the pioneer-dominated plant community has changed in relation to the introduction of new species, and the evolution of the channel and its flood plain.

Day 1

Grass Valley summit to Hanksville

The trip proceeds south from Salina via Interstate 70, U.S. Highway 89, and Utah State Highway 24 (U-24). The route passes along the transition between the Basin-and-Range and Colorado Plateau structural provinces, crossing the Sevier and Paunsagunt Faults, two large down-to-the-west normal faults of Neogene age. The detailed log begins at Grass Valley summit, the divide between the Fremont River and the Sevier River. For additional information on the geology along the route, see Oaks, 1988.

Utah State Highway 24

Milepost 42— Summit at elevation 8385 feet; pass between Parker Mountain, to the south, and the Fish Lake Plateau to the north. This is the drainage divide between the Sevier River, tributary to the Great Basin, and the Fremont River, tributary to the Colorado. To the north at 9:00 on the summit of Fish Lake Plateau is the south end of the graben that contains Fish Lake. At 300 feet, it is one of the deepest natural lakes in Utah, and a source of the Fremont River. The north end of the lake is partly dammed by glacial moraine, suggesting that it could have been the source of Pleistocene glacial outburst floods on the Fremont.

In the near distance, the Fremont Valley cuts between two lava-capped plateaus, with summits near 11,000 feet: Thousand Lake Mountain to the left and Boulder Mountain to the right. The two northern peaks of the Henry Mountains are visible to the east in the far distance; Mt. Ellen to the left and Mt. Pennell to the right. The Henry Mountains were the last mountain system to be placed on the map of the United States. They were first described by G.K. Gilbert in his seminal work on geomorphology and igneous intrusions (Gilbert, 1877). Hunt, et.al. (1953) conducted the first detailed mapping of the Henry Mountains between 1935 and 1939 (Hunt, 1977).

Milepost 47— Road cut exposes bouldery lahar in the volcanics. The source of the volcanics, as well as some on Thousand Lake and Boulder Mountains, is in the Marysvale calderas 35 miles to the west, showing that at least the earliest eruptions, dated at 23 million years (Mattox, 1991), predate offset on the Paunsagunt and Thousand Lakes Faults.

Milepost 48— Begin descent into Rabbit Valley. Eastward across the valley is the west face of Thousand Lake Mountain, the escarpment of the Thousand Lake Fault, considered to be the western margin of the Colorado Plateau. Note the horizontal lava cap and the patches of the more resistant Triassic and Jurassic sandstones peeking through landslide-mantled slopes.

Milepost 50— U-24 crosses a peculiar crescent-shaped valley. A large spring which emerges from the volcanic rock on the western margin feeds one of several fish-farming operations of the upper Fremont River.

Milepost 51— Entering the town of Loa. Loa was named after the Hawaiian mountain, whose gently sloping flanks bear some resemblance to the volcanic slopes to the west and north. **At the south end of town, leave U-24 and continue south** on Main Street. Set odometer to zero.

Mile 0.8— End of pavement. Continue on graded county road.

Mile 2.1— Road forks, **TURN LEFT**.

Mile 2.7— Outcrop of welded Osiris Tuff whose joint blocks weather into large monoliths.

Mile 3.9— Regain pavement and cross the Fremont River. The river here leaves the valley, and continues south in a canyon cut into the north-eastward dipping volcanics. G.K. Gilbert recorded this feature in his field notes of July 12, 1875, and puzzled over whether the course was antecedent or superposed (Hunt, 1988, p. 34).

Mile 5.0— The road ascends the alluvial slope east of the river. Wayne Wonderland airport to the left. To the right is a small knoll underlain by horizontally bedded sand and gravel mapped as Pleistocene Fremont River terrace deposits by Smith, et. al. (1963). The sediment is similar to Tertiary gravel interbedded with the volcanics elsewhere in Rabbit Valley, and the hill is likely a remnant of Tertiary basin fill.

Mile 6.0— **Junction with U-24; TURN RIGHT and continue southeast** toward Bicknell.

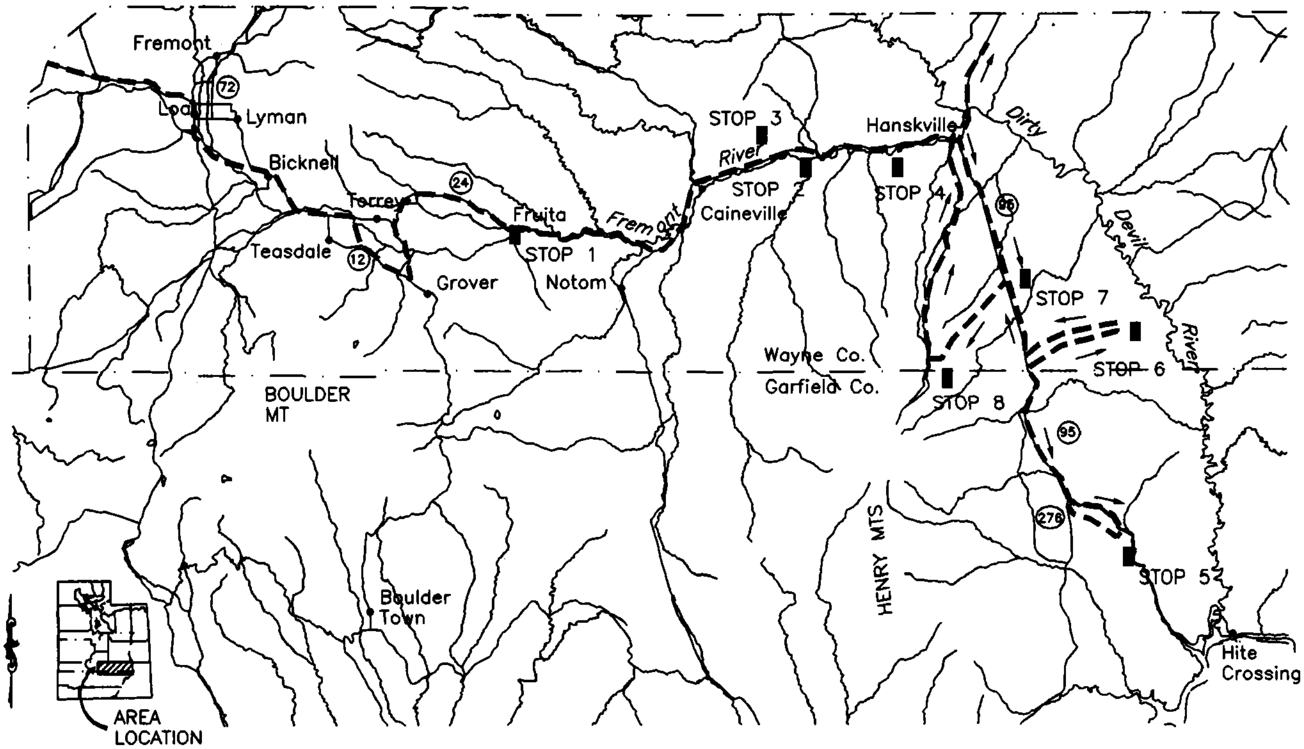

Figure 1. Map of field-trip route in area of Capitol Reef National Park and the Henry Mountains, with stops shown.

Milepost 59 on U-24—At 3:00 across the valley to the west is the mouth of the canyon by which the Fremont River returns to the valley. As the road turns eastward, the cliffs ahead expose horizontally bedded Triassic Wingate Sandstone. At the mouth of Sand Creek is a tilted block of Navajo Sandstone (Ss) within the Thousand Lake Fault zone.

Milepost 60— To the right, the Beard Oil Tanner #1-27 in 1990 penetrated the Carmel-Entrada Formation (Fm) at a depth of 730 feet beneath interbedded alluvium and volcanics. Offset of the Chinle Fm across this part of the Thousand Lake Fault is 2,500 feet. Faulting began in the early Miocene and continued through at least the Pliocene. There is no clear evidence for late Pleistocene or Holocene offset (Everitt, 1995). Enter Bicknell.

Milepost 62— To the south at 2:00, the Fremont River meanders through a broad marshy valley called the Bicknell Bottoms. The low gradient suggests ponding by either structural deformation or backwater from downstream glacial dams. Springs emerging from the toe of the volcanic slopes across the valley provide a year-round base flow of about 100 cfs.

Milepost 63— Cross the Thousand Lake Fault and enter what G.K. Gilbert called the "Red Gate" (Hunt, 1988). The lower Triassic Moenkopi Formation is exposed at river level north of the river, forming red cliffs capped by the resistant Shinarump Member of the Chinle Fm (fig. 2). Notice how much larger the Fremont River is here than upstream from the Bicknell Bottoms.

Milepost 66— Mt. Ellen in the distance at 1:00. The first well-defined gravel-capped river terraces are on the right.

Milepost 67.5— Bridge over Fremont River. Drilling for a proposed dam in 1992 showed 35 feet of alluvial valley fill beneath the floodplain, with an inner buried canyon an additional 45′ deep buried beneath the west valley margin (fig. 3).

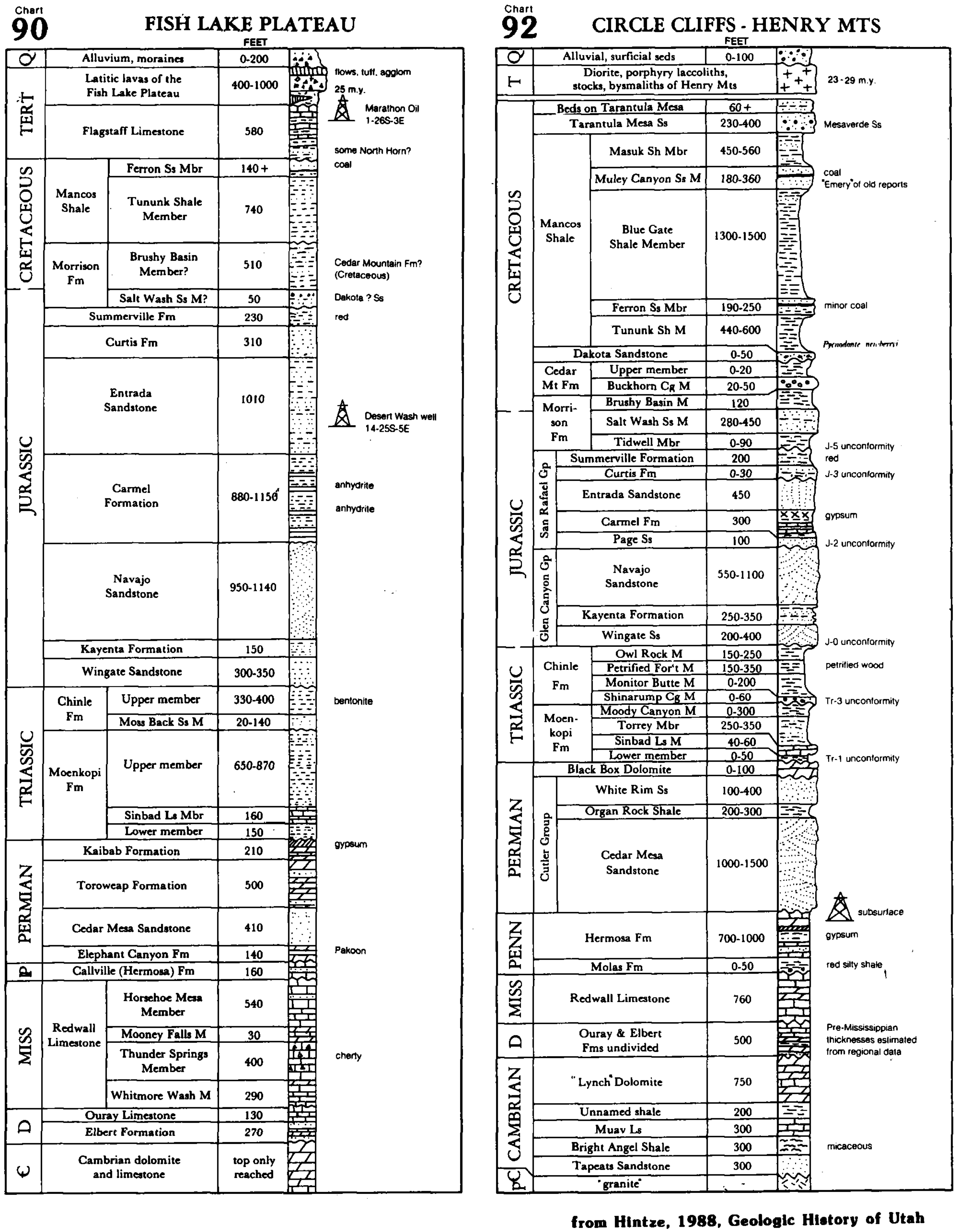

Figure 2. Stratigraphic columns for Fish Lake Plateau and the Circle Cliffs-Henry Mountains area.

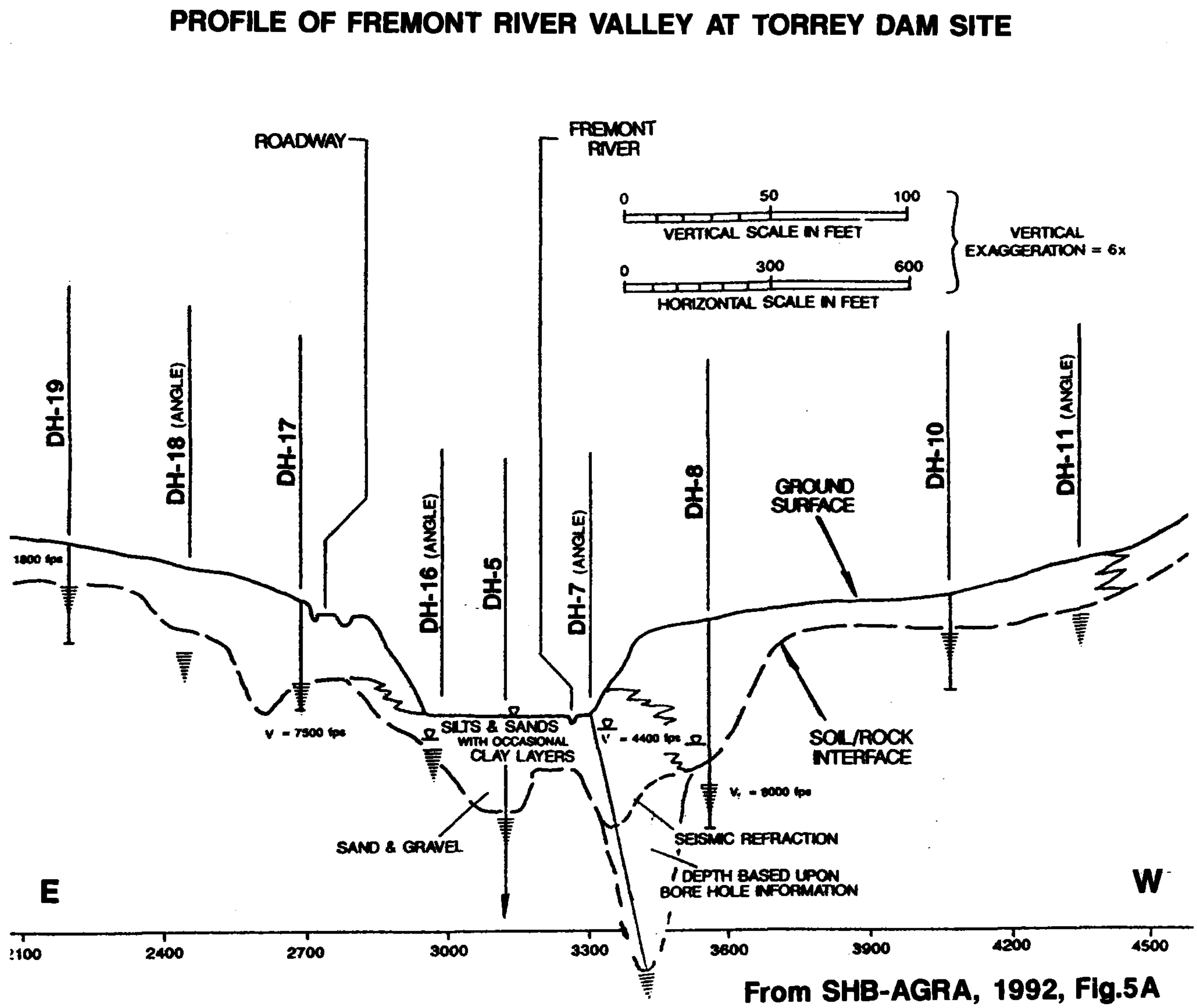

Figure 3. Profile of Fremont River valley at Torrey dam site.

Continue through Torrey, and **TURN RIGHT** on 300 East, the first road past the post office. Set odometer to zero.

Mile 1.0— Descend into the Fremont valley through a cut in the Moenkopi Fm.

Mile 1.4— Abandoned Garkane hydropower station and penstock is west across the valley behind the quarry. Ahead to the south, the narrows flanked by bedrock was studied as a potential dam site in 1987. The modern valley here is of latest Pleistocene or Holocene age (fig. 4). The Pleistocene valley lies to the south of the modern valley beneath the gravel terrace (Qat of Billingsley and others, 1987).

Mile 1.6— Pleistocene valley fill exposed in road cut to the right.

Mile 1.7— Bedrock exposed to the left of the road separates the Holocene valley on the left from the Pleistocene valley ahead.

Mile 2.7— **TURN LEFT on County Road 3262.**

Mile 3.7— Road parallels the SE-trending Teasdale anticline, believed to be a Laramide (late Cretaceous to Eocene) structure. Moenkopi Fm crops out on the left. The ridge of fractured Navajo Ss on the right, now called the "Cockscomb," is Gilbert's "White Crag" (Hunt, 1988, p. 37).

Mile 4.7— Road forks, **BEAR RIGHT**.

Mile 5.7— **TURN LEFT on U-12.** The lumpy, bouldery terrain is Flint and Denny's (1958) Carcass Creek Drift.

Mile 6.4— The sloping surface is the glacial outwash fan of Fish Creek, graded to the Pleistocene Fremont River about 100 feet higher than the present river (Flint and Denny, 1958). Carcass Creek Drift, of possible Bull Lake age, is exposed beneath the outwash along the river. At this location, therefore, a glacier once dammed the Fremont River and pushed it northward.

Mile 7.7— Bridge over Fremont River. The basal Sinbad Limestone Member of the Moenkopi Fm exposed in riverbed just downstream.

Mile 10.2— **Return to U-24** at milepost 70. **TURN RIGHT** toward Capitol Reef National Park.

Milepost 74— Capitol Reef National Park boundary. The trip through the Park provides a traverse through the Mesozoic stratigraphic section (fig. 2).

Milepost 75— SE-trending high angle fault and basalt dike parallels the highway to the left.

Milepost 82— Highway returns to the Fremont River. **TURN RIGHT** to Park headquarters at Fruita.

STOP 1: Capitol Reef National Park Visitor Center. The relief model shows the interesting topographic features developed on the Water-pocket Fold, including superposed stream courses entrenched in sandstone canyons.

Milepost 83— Entering the narrows of the Wingate Fm. The locally mild climate created by the narrow canyon favored development of fruit orchards, which are now operated by the Park as a reserve of classic varieties.

Milepost 85— Navajo Ss at river level. Basalt boulders on two terrace levels. In 1960, the Utah Department of Transportation (UDOT) drilled three borings for Utah Highway 24 structure D235 over the Fremont River near Fruita (UDOT files). Bedrock was encountered at a maximum depth of 15 feet, 10 feet below river level. Because these borings do not provide a complete traverse across the valley, the maximum thickness of fill may be greater than 15 feet.

Near *Milepost 86.* Navajo Ss penecontemporaneous deformation. The canyon meander cutoff on the right, and waterfall on the left were constructed by the Utah Department of Transportation during highway construction in the 1950's. Two terrace levels are capped by basalt boulder gravels.

Near *Milepost 87* and thereafter: Proceeding up-section through Carmel Fm, Entrada Ss, thin green Curtis Shale and the thinly bedded chocolate Summerville Fm, overlain unconformably in places by Pleistocene terrace gravel.

Milepost 90— Salt Wash Sandstone Member of the Morrison Fm is overlain by the distinctive purple claystone of the Brushy Basin member. Two river terrace levels are present.

Milepost 93— Highway enters strike valley in the Tununk Shale Member of the Mancos Fm. Eastward dip increases toward the Caineville monocline. Turnoff to the USGS gaging station "Fremont River near Caineville" on the left.

Milepost 94— The dark gray Tununk directly overlies the green-gray shale of the Brushy Basin Member of the Morrison Fm. The usually intervening Dakota Ss is absent (fig. 2).

Milepost 95— U-24 bridge over the Fremont River and the Caineville Diversion where the Caineville Irrigation Company takes its water. In 1980, investigation for an earthfill dam in the narrows just upstream showed the thickness of the alluvial valley fill to be 50 feet (Palmer-Wilding, 1981).

Milepost 98— Highway bears right through the Caineville Reef, a hogback of Ferron Ss Member of the Mancos Fm folded upward on the steep western limb of the Henry Mountains structural basin. Return to the Fremont River valley at Caineville. A review of drillers' logs of water wells in the town of Caineville show bedrock at a maximum depth of 60 feet below terrace level, or about 45 to 50 feet below river level (Everitt, 1984).

Milepost 100— The Fremont River valley passes between the escarpments of North and South Caineville Mesas, the "Blue Gate" of G.K. Gilbert (1877). At the axis of the Henry Mountains structural basin are about 2,000 feet of horizontally bedded Blue Gate Shale Member of the Mancos

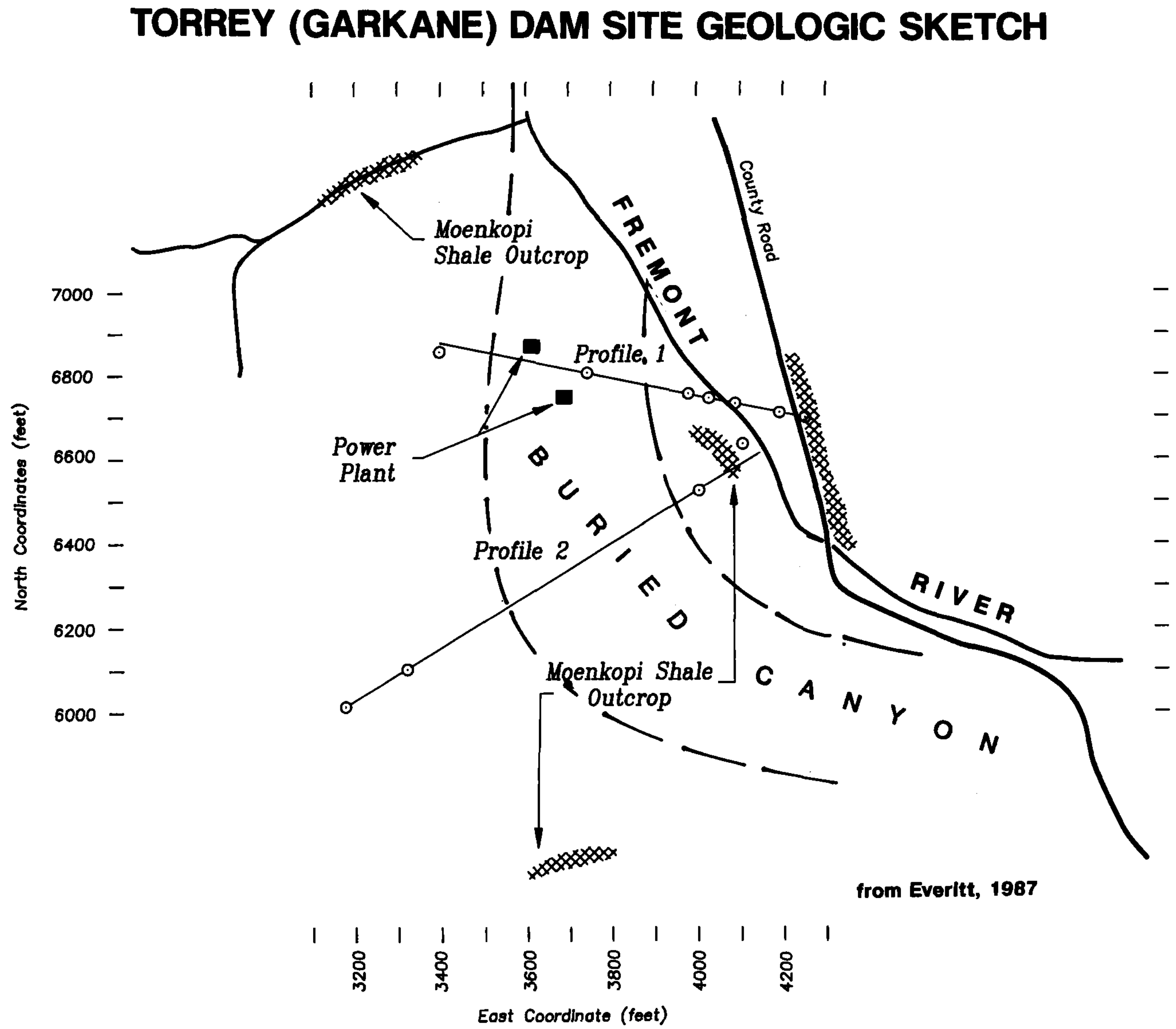

Figure 4. Torrey (Garkane) dam site geologic sketch.

Fm, capped by the Emery Sandstone Member.

Milepost 101— Luna Mesa store; the butte ahead on the left is capped by Fremont River gravel, Howard's (1970) terrace 3a.

Milepost 104— To the left are asymmetrical ridges in the Blue Gate Shale, some with vertical faces on the northeast side. In 1876, G.K. Gilbert observed these, and postulated an aeolian origin (Hunt, 1988, p. 214).

Milepost 105— Ascend the dip slope of the Ferron Sandstone with outcrops of white and tan sandstone interbedded with coal. This marginally economic coal zone was open-pit mined briefly in the 1980's at the Factory Butte coal mine about 15 miles along strike to the north.

Mile 106.1— Road junction. **TURN RIGHT** (south) on dirt road which climbs to the top of Howard's (1970) terrace 3a. Proceed 0.6 mile to overlook just past TV relay.

STOP 2: Overlook of the Fremont River valley, terrace levels, and the badlands around the Caineville mesas (Howard, Anderson, Godfrey). Drilling and seismic refraction traverses for a proposed dam on the Fremont River downstream from

BLUE VALLEY DAM SITE
PROFILE 2, DRILL HOLES AND SHOT POINTS

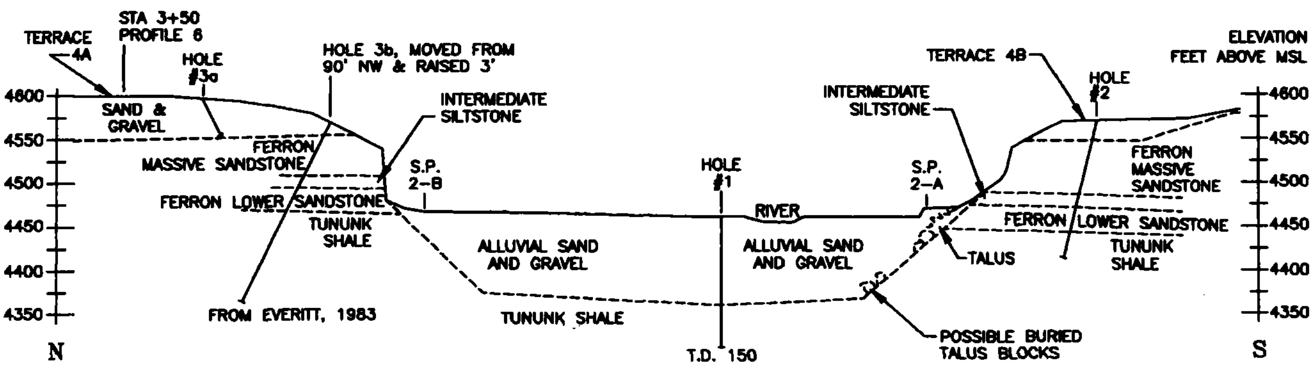

Figure 5. Geologic profile of Blue Valley dam site, with drill holes and shot points.

Caineville (Everitt, 1983) showed a thickness of 99 feet of alluvial fill beneath the flood plain (fig. 5). The site is in a canyon cut into the Ferron Sandstone Member of the Mancos Formation. The canyon rim is capped by gravel mapped as terrace levels 4a and 4b by Howard (1970). The extensive surface of terrace 4a conceals beneath it, to both the north and south of the modern canyon, filled canyons similar in width to the modern canyon, although not as deep.

Return 0.2 mile to test pits exposing soil profile of terrace 3a.

Return to Highway 24 and TURN LEFT (west) toward Caineville.

0.3 miles west of *Milepost 105*—East side of hill. **Turn off on track to right**, 0.2 mile to old highway, 0.5 mile to badlands. Or, as an alternate, turn off highway at mile 105.1 to the fluted wind towers at the dirt bike jamboree area.

STOP 3: Mancos Shale badlands and sites of wind erosion and soil creep (Godfrey); badlands modeling (Howard); and runoff monitoring (Anderson).

Return to U-24 and proceed east toward Hanksville.

Milepost 106.2— Highway descends the dugway through the Ferron Sandstone hogback and returns to the river valley. The Tununk Shale now at river level.

Milepost 108— The ghost town of Giles, abandoned in 1907, is across the river to the right. To the left between here and milepost 109 are the remains of an abandoned irrigation ditch with dead cottonwood trees along it. The trace of the canal is marked by pink silt from the Fremont River, which contrasts with the gray, residual soil of the Tununk.

Milepost 109— Blue Valley is a strike valley in the Tununk shale.

Milepost 110— Dakota Sandstone with interbedded coal ahead on the left. The basal Mancos consists of an oyster shell reef (*Gryphaea*) from 2 to 5 feet thick. (Possible stop, highway borrow pit on left.)

TURN RIGHT 0.2 mile past milepost 111 and proceed 0.1 mile on dirt track to abandoned well.

STOP 4: Fremont River flood plain and location of 1983 traverse of Fremont River flood plain and its vegetation (Everitt).

Milepost 111.5— Variegated shale of the Brushy Basin Member is at river level, capped by the Dakota Ss. Note the tilted slump block of Brushy Basin on the left.

Milepost 113— Extensive river terraces on the Brushy Basin are capped by Fremont River gravel. As the road goes over the rise, Howard's (1970) terrace 4b is on the right.

Milepost 114— Outcrops of Salt Wash Ss Member of the Morrison Fm are at river level ahead.

Milepost 115— Summerville Fm on the left, capped by the massive basal gypsum of the Morrison. Note the interbedded gypsum, with gypsum-filled fractures at various angles. The Fremont River on the right is aggrading above the Hanksville diversion dam, which has provided grade control since at least 1947.

Milepost 116— Fremont River bridge, entering Hanksville. In 1965, four borings were drilled here (structure F116, UDOT files). The deepest encountered bedrock beneath valley alluvium to a depth of 27 feet, 20 feet below river level. Because the bridge is near the south margin of the valley, this should be regarded as a minimum thickness of alluvial fill. A review of water wells in the town of Hanksville suggests a maximum of more than 100 feet of alluvial fill.

The highway is on a surface that is believed to have been the Fremont River flood plain at the time of settlement in the 1870's. During a series of floods beginning in the 1890's, the river cut the present channel 15 to 20 feet below the old flood plain (Hunt and others, 1953), and since about 1940 has been reconstructing a new floodplain at this lower level. North across the river at 9:00 is a little anticline in the Entrada Fm. The pinching out of beds at the top of the anticline indicates active folding during deposition.

END OF DAY 1

Day 2

Henry Mountains Piedmont near Hanksville

Begin at Hanksville and **proceed southeast on U-95** from milepost 0.

Milepost 1— The rolling, sandy country is underlain by the Entrada Fm. The Entrada forms sandstone pillars surrounded by moats.

Milepost 2.5— Highway bends left around a pediment remnant (Godfrey, 1969), an ancient channel of Bull Creek. The light gray gravel is diorite porphyry derived from the Henry Mountains. At 2:00 are the Henry Mountains. Mt. Ellen is the sharp peak on the right and Bull Mountain is the lower sharp peak to its left. Modern Bull Creek flows northward from the basin between the two.

Three types of surfaces can be identified: (1) gravel-capped pediments, (2) alluvial fans, and (3) stripped benches on the resistant sandstones. The pediments and alluvial fans here slope north and east away from the mountains, whereas the stripped benches are west-facing dip-slopes on resistant sandstone units. The entire area between the mountain front and the Fremont River is referred to as the "piedmont." A pediment is a primarily erosional segment of the piedmont where bedrock is beveled by running water, so that bedding is truncated. An alluvial fan is a depositional segment of the piedmont (Godfrey, 1969, p.3).

Mile 3.5— The valley of Dry Valley Creek is a former course of Bull Creek into which Bull Creek was artificially diverted in the 1950's to keep it from flooding Hanksville.

Milepost 4— On the left are four gravel-capped pediments radiating from the northern Henry Mountains.

Milepost 8— To the east at 10:00 is Sorrell Butte, a pediment remnant capped by Bull Creek gravel, one of the oldest and highest remaining levels of the Henry Mountains pediments. It is flanked by radiating secondary pediments.

Milepost 10— Sawmill Basin road on the right.

Mile 12.8— Highway crosses Granite Wash which heads on the eastern slope of Bull Mountain. Coppice dunes (sand mounds of Everitt, 1980) are occupied by Brigham tea (*Ephedra torreyana*). Exposures in cross-section show that these are not traveling dunes, but layered accumulations of drift sand accreting with the growth of individual bushes.

Milepost 13— Bull Mountain is at 3:00 (southwest). Hunt, et.al. (1953) classified it as a bysmalith—a laccolith (a floored, domed, igneous intrusion) with a faulted distal end. Note the sedimentary beds turned up around the base at the distal end, and the pattern of radiating fins on the summit.

Milepost 16— Garfield County line. To the west at 4:00 is a good view of Bull Mountain. In the foreground is a hogback of Summerville

Fm capped by the Salt Wash Sandstone Member of the Morrison Fm. Beyond, at the base of Bull Mountain, is horizontally bedded Salt Wash Ss.

Milepost 17— Bridge over Poison Spring Wash. The road cuts through a pediment with a cap of porphyry gravel channeled into the underlying Entrada Fm.

Milepost 21— Mt. Pennell is at 2:30; Mt. Hillers at 2:00. The Little Rockies (Mts Holmes and Ellsworth) are in the distance at 1:00.

Milepost 23— Highway descends to the valley of North Wash. Henry Mountains gravel caps pediments on the Navajo Sandstone.

Milepost 26— Junction of Highway 276 to Bullfrog. Continue east on Highway 95 into the canyon of North Wash.

Mile 29.5— Contact of the Navajo Ss where with the underlying Kayenta Fm.

STOP 5: Alcoves formed at the Kayenta-Navajo contact by groundwater sapping (Howard).

Return northward on U-95, to just north of the Garfield/Wayne county line.

Mile 15.7— **TURN RIGHT** on graded road toward Burr Point, 11 miles.

STOP 6: Burr Point, and overlook of the Dirty Devil River Canyon. Review of Triassic stratigraphy, terrace formation, abandoned and filled canyons, and riparian vegetation (Howard, Everitt).

Milepost 10— Gravel pit on the right (east).

STOP 7: Gravel Pit with an exposure of a soil with a well developed gypsiferous carbonate horizon.

Proceed north 0.2 mile on U-95 and **turn left** (southwest) on the Saw Mill Basin road. Set odometer to 0. Mt. Ellen is straight ahead. Bull Mountain is at 11:00. At the base of Bull Mountain are flat-lying sedimentary strata of the Salt Wash Member of the Morrison Fm. Just in front of and to the left of Mt. Ellen Peak is Horseshoe Basin, which is thought to be the source of some of the landslide debris around the north slopes of the range and the north side of Bull Mountain. At 1:00 is Table Mountain, one of the radiating laccoliths of the Ellen group.

Mile 2.4— Road climbs onto gravel-capped pediment surface.

Mile 2.7— Road forks: **BEAR LEFT** toward Granite Ranch.

Mile 3.2— View SSW toward the mouth of Bull Creek Canyon along a broken pediment surface, the Cottrell level of Godfrey (1969), to the few remnants of higher, older surfaces to the left. To the right is the head of a drainage in the process of eroding headward into the Cottrell pediment and slowly beheading it.

Mile 5— Road rises onto a higher sublevel within the Cottrell group of pediments. At 2:00 is a remnant of a higher ancient pediment at the Sorrell Butte level. This remnant is flanked by an apron of secondary pediments cut on the Mancos shale.

Mile 5.8— Road forks. **Take the jeep track to the RIGHT** and continue up the pediment surface. To the left across the draw is the apron of landslide debris at the foot of Bull Mountain, which appears to be graded to Horseshoe Basin.

Mile 6.5— The toe of the landslide with a group of large porphyry boulders with tafoni (cavernous weathering).

STOP 8: Pediment overview and review of erosion and deposition process (Godfrey). To the north is visible the general westward dip of the beds on the east limb of the Henry Mountains Basin and in the distance, the San Rafael Swell and the Book Cliffs. To the northeast is the canyon of the Dirty Devil River. If the day is clear, the LaSal Mountains may be visible 90 miles to the east.

Proceed westward across the pediment surface. Note the contrast between the rounded boulders in the pediment gravel and the angular and irregular boulders of the landslide.

Mile 7.0— Cross a small drainage, which exposes the pediment gravel in cut banks.

Mile 7.4— Rejoin the Sawmill Basin road and **TURN RIGHT** (north). The road descends from the Cottrell pediment onto the Fairview pediment. The modern channel of Bull Creek is to the left.

Mile 8.0— Proceed downstream along the Fairview pediment, which lies in a valley eroded into the Cottrell pediment. Remnants of the Cottrell pediment are on both sides of the lower, younger pediment. Exposures show 15 to 20 feet of gravel overlying Mancos Shale.

Mile 9.0— To the right are badlands eroded in the Brushy Basin Member, with remnant caps of pediment gravel. Fairview Ranch is straight ahead.

Mile 10.0— Road junction and Fairview Ranch. **Continue north toward Hanksville.**

Mile 11.2— Proceed north on the Fairview pediment with outcrops of Brushy Basin Member poking through here and there.

Mile 11.6— Adams Butte to the northwest at 10:00 is a remnant of Brushy Basin shale. Post-pediment slope retreat has formed a moat around the base of the butte.

Mile 12.4— Cattle guard—we are now at the distal end of the local branch of the Fairview pediment. Distally thinner gravel forces groundwater to the surface here, leaving an efflorescence of thenardite: anhydrous sodium sulfate. A slightly higher, older branch of the Fairview pediment is at 2:00.

Mile 13.0— Road rises on the dip slope of the Salt Wash Ss. The pink sandy soil is derived from the Entrada Fm. Drift sand forms coppice dunes occupied by Brigham tea.

Mile 15.3— Road descends to the flood plain of Bull Creek. The gray, silty alluvium is derived largely from the Mancos Shale. The nearby arroyo with the young cottonwoods growing in the bottom is the active Dry Valley distributary of Bull Creek. In the distance to the northwest, old cottonwoods mark the course of the abandoned, pre-1950 Hanksville distributary. Although short, discontinuous sections of arroyo were present as early as 1850, the present continuously deep arroyo did not appear until after 1910 (Everitt, 1979).

Mile 16.0— Bridge over the Dry Valley branch of Bull Creek.

Mile 16.5— At 11:00 are bluffs formed by the Summerville Fm and capped by the basal gypsum of the Salt Wash Member of the Morrison.

Mile 17.0— The greenish-gray marine shale is the Curtis Fm, which immediately underlies the Summerville.

Mile 18.6— At 10:00 the Curtis unconformably overlies the Entrada, which is gently folded.

Mile 22.2— Hanksville, and the junction of U-24 at milepost 117.

Continue north on U-24.

Milepost 118— Fremont River terraces here are capped with gravel mostly derived from Henry Mountains porphyry, transported northward by ancestral Bull Creek.

Mile 119.5— Highway crosses the Dirty Devil River just downstream from the confluence of the two main branches. The Fremont River enters from the left (south) and Muddy Creek enters from the right (west). In 1973, five borings were drilled to investigate the bridge foundation (structure C656, UDOT files). The bridge abuts the north side of the valley. The thickness of alluvial fill increases southward from the north side of the valley to a maximum of 53 feet (50 feet below river level) at the south end of the bridge. Because the borings do not span the entire valley, this thickness should be regarded as a minimum.

Milepost 120— Road climbs to Airport Bench. Left at 9:00 are Factory Butte and the Caineville mesas, with the high plateaus in the distance.

Milepost 122— Castles of Entrada Ss on the left with basal moats formed by wind scour.

Milepost 123— Scenic turnout, optional stop. San Rafael Swell, distant left, is the steep east face of an asymmetrical anticline of Laramide age. The light-colored rock forming the principal hogback is the resistant Navajo Ss. View of Henry Mountains to the south and the high plateaus to the west.

END OF LOG—The route continues northward along the foot of the San Rafael Swell via U-24 to Interstate 70 and U.S. Highway 6, returning to Salt Lake City and the Basin-and-Range Province via Soldier Summit. For descriptions of geologic features, see Oaks, 1988; Laine, et.al., 1991, and Rigby, 1976. For general historic information, see Midland Trail Association, 1916; and Van Cott, 1990.

Wind Erosion of Mancos Shale Badlands—Part 2

ANDREW E. GODFREY

INTRODUCTION

When G.K. Gilbert crossed the Mancos Shale badlands homeward bound on election day, 1876, he wrote in his notebook (Hunt, 1988, p. 214):

> "There is a very curious phenomena (sic) of badlands across the river. At a score of places I can see them vertical on the NE side and sloping on the opposite. The prevailing wind must be from the side that has the slope. Can that in some way account for the phenomenon?"

Recent research by Godfrey (1997a) has determined that the phenomenon observed by Gilbert is caused by wind erosion. However, it is caused by vacuuming rather than by the tractional forces so well known in sand deserts.

The badlands are underlain by the Blue Gate Member of the Mancos Shale. Paralithic soils developed on this shale have a gypsum-cemented crust averaging 1.2 cm thick overlying randomly oriented silt- to sand-sized shale chips.

This area averages about 13 cm of precipitation a year.

THE PROCESS

Wind erosion of Mancos Shale badlands occurs only on the lee sides of ridges, not the windward side nor along flats when the soil curst is undisturbed. Preceding the passage of cold fronts, this area receives gusty southwest winds. There is an average of over ten such fronts a year, mainly during the months of March, April, and October.

Above the tops of the badland ridges the wind can explosively accelerate from about 7 ms^{-1} up to 22 ms^{-1}. This rapid acceleration of the wind causes a barometric-pressure drop that lasts one second or less. This pressure drop occurs on the upper portion of the lee slopes. The pressure drop can be up to 1.27 mm Hg, but averages 0.76 mm Hg. This drop can be attributed to two factors: the Bernoulli effect and the expansion of a turbulent zone on the upper lee side of ridges that can be shown by tests with streamers and dust.

During the short-lived interval of local air-pressure decrease, the soil atmosphere below the crust remains at ambient levels. This pressure difference can produce a lifting force of as much as 1.7×10^{-2}N, nearly twice the unit force of gravity on the crust, which averages 0.88×10^{-2}N and ranges from 0.62 to 1.5×10^{-2}N.

RESULTING FEATURES

This vacuuming process produces distinct erosional features on the lee sides of badland ridges. The smallest feature is the cavity left by the removal of a crustal polygon (fig. 6). Removal of the cemented crust exposes the underlying shale chips to be blown away later.

Continuation of the process forms micro-cirque features near the crests on the lee sides of ridges. Some have flat floors, in others the normal slope of about 40 degrees extends up to the vertical cliff (fig. 7). In the largest of these features, the downwind-facing cliff can attain a height of nearly 10 m.

A second feature that can be produced by the vacuuming process is a closed depression. These depressions are up to 1 m deep and 10 m in diameter (fig. 8). Some are at the bases of downwind-facing cliffs, others are near the crests of ridges. The floors of these depressions are smooth and flat, which suggests that they are being partially filled by sediment washed from surrounding slopes. These closed depressions are not formed by solution as there are no soluble rock types for several thousand feet stratigraphically beneath this area.

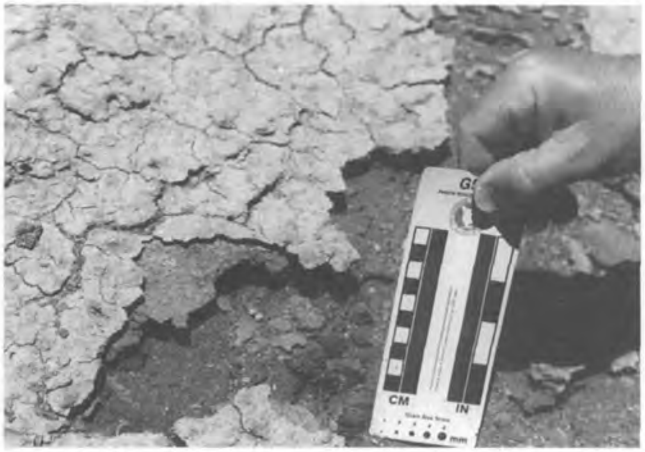

Figure 6. Removal of individual polygons of crust. The underlying soil of shale chips is exposed.

Figure 7. One of the micro-cirques along a ridge crest. The southwest winds blow from right to left. Cliff is about 1 m high.

Figure 8. Closed depression downwind of a cliff that has been breached by headward erosion of a micro-cirque. Wind direction is toward the camera. Note person for scale.

Long-term Measurements of Soil Creep Rates on Mancos Shale Badland Slopes—Part 3

ANDREW E. GODFREY

INTRODUCTION

Outcrops of Cretaceous Mancos Shale form a broad belt across the Colorado Plateau of southeastern Utah and southwestern Colorado. They are a major source of salinity and sediment to the Colorado River (Schumm and Gregory, 1986). Howard (1994a, b) used simulation models to argue that sediment production was limited by detachment rather than by transport.

This report summarizes a 30-year study conducted to determine the rate of downslope movement of surficial soil developed on the Mancos Shale near Caineville, Utah (Godfrey, 1997b). Other segments of the investigation, covering about a decade, studied the effects of aspect, slope position, seasonality, and depth of soil movement.

PROCEDURES

Seven sites were established. One was maintained for 30 years, and measured sporadically. Three were maintained for a decade and were measured mostly in June and November. Three others were maintained for almost seven years and were only measured at the beginning and end of the seven-year period.

Each site consisted of between 16 and 24 nails, 9 cm long, inserted vertically into the soil between benchmarks placed along the contour of the slope. Spacing of the nails was either 0.3 or 1.5 m. Benchmarks consisted of rods 1 m long driven vertically about two-thirds of a meter into the soil.

Measurements were made along the slope from a point directly below a string stretched between two benchmarks and the point where the nail met the soil surface. Average downslope distances and their standard deviations were then calculated for each measurement time at each site. These average distances were then plotted, and the linear regression computed to determine the average soil-movement rates.

RESULTS

The 30-year study showed an average downslope rate of 2.7 cm/yr on slopes averaging 35 degrees.

Data from one of the seasonally measured sites (see fig. 9) indicate several episodes of more rapid downslope movement. These steps occurred during the winters of 1985 and 1988, whereas smaller steps occurred during the winters of 1983 and 1991. Correlation of these episodes with precipitation records from the Hanksville weather station, 20 km to the east, indicates that the larger steps occurred during winters when there were two or more consecutive days of at least 6 mm of precipitation. The smaller steps occurred when the two consecutive days had between 2.5 and 6 mm of precipitation for the day with the lesser precipitation.

A Student's T test comparing movement rates on north- and south-facing slopes showed no significant difference in the populations at the 95 percent confidence level. The comparison was made for the period of five years before the north-facing site was disturbed.

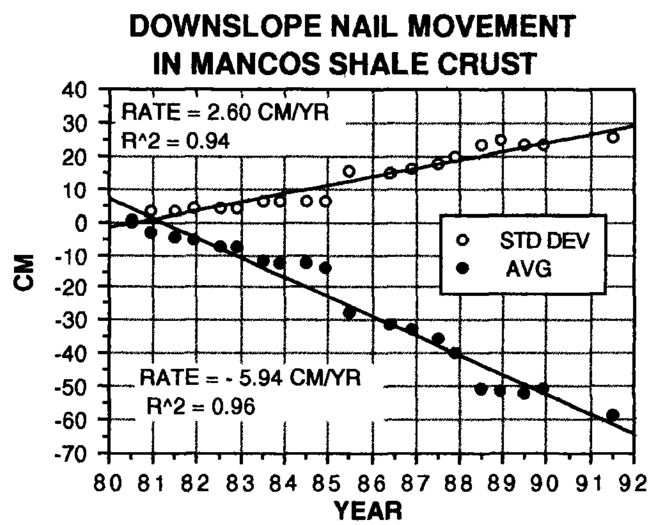

Figure 9. Graph from one of the study sites near Caineville, Utah. It shows the average downslope distances of 20 nails at the times of measurement and the standard deviations of those distances. Regression lines through both were used to determine their rates. Note that the standard deviation of the set of nails increases over time, which indicates increasing distances between higher and lower nails on the slope.

Slope position appears to be an important factor controlling movement rates, as indicated by the sites measured only at the beginning and end of a seven-year period. The site between 1 and 2 m below the ridge crest moved at an average rate of 0.7 cm/yr. At the same time, sites 5 and 10 m below the ridge crest moved at an average rate of 4.1 and 4.5 cm/yr. A Student's T test between the upper and middle sites indicated there were two separate populations at the 99 percent confidence level.

Figure 9 shows that the spread of the nails, as measured by the standard deviation, increases with time. For all the sites the rate of increase of the standard deviation is between 35 and 46 percent of the average downslope distances the nails had moved at any given time. This spread of the nails indicates that downslope movement of the soil surface occurs as independent slices up to a few meters wide, with each slice moving independently. The relatively large spread in the distances the nails move helps explain why there is no significant difference in the rate of movement between north- and south-facing slopes.

The nails rotated in a downslope direction as they moved downslope. This indicates that a shallow surface layer of the soil is involved and that lower layers of the soil either are stable or move quite slowly.

Vegetation and Geomorphology on the Fremont River—Part 4

BEN EVERITT

INTRODUCTION

Dynamic sand-bed rivers such as the Fremont River of southern Utah provide a fruitful area for the study of the relationships among the variables of climate, hydrology, geomorphology and riparian vegetation. The changing survivorship of different pioneer species is recorded on flood bars of different ages.

PHYSIOGRAPHY

During the last century the Fremont River passed through an episode of arroyo cutting. Between 1896 and 1916 a series of floods gutted the valley, forming a wide braided channel which has destroyed most traces of the former narrow sinuous one (Wooley, 1946; Hunt, et.al., 1953; Graf, 1983; Webb, 1985). The present river is a product of the gradual shrinking of the channel and construction of a flood plain inset within the 1896 arroyo, mostly since 1940 (Everitt, 1995).

The valley floor and floodplain can be subdivided into physiographic units for the purposes of describing topography and vegetation. In figure 10, I have used the classification of Osterkamp and Hupp (1984, fig. 1). The *channel bed* (CB) carries the low flow, when there is any, and is wet most of the time. *Depositional bars* (DB) are ephemeral features in or adjacent to the channel bed, formed of newly deposited sediment, and unvegetated except by sparse annuals and seedlings. The Fremont presently has an *active channel shelf* (AS) which is a composite of many flood-deposited treads separated by steps and rising 0.9–1.2 meters above low water. The boundary between the channel shelf and the more horizontal surface of the *active flood plain* (FP) is a matter of judgement. The floodplain surface undulates between *flood bars* (FB) and *swales* (FS), with a relief of 0.3–0.6 meter. Behind the active flood plain are remnants of *terrace* (T), the flood plain abandoned in 1896. The terrace is about 3 meters above the active flood plain and separated from it by an erosional scarp. The substrate is friable fine sand with minor silt, with clay locally in the swales.

The relative area occupied by the various physiographic subdivisions of the flood plain has changed as the modern valley has evolved. The active flood plain with its bars and swales provides a variety of habitats for vegetation. It is mostly younger than about 1940 (Graf, 1983); the oldest woody plant found so far (tamarisk) dates from the 1950's (Everitt, 1995). The habitat available for colonization is evolving as the river evolves. The present flood plain is undoubtedly quite different from the braided channel of 1940, with respect to elevation, time subject to inundation, propensity to scour, stage versus velocity, and elevation above normal water table.

Graf (1983) presented a model of the Fremont River as one which alternates between two states: a process-dominated state, in which channel morphology is principally a function of discharge; and a form-dominated state, in which the geometry of channel and flood plain present more inertia, and exert feedback to the flow. The Fremont is evolving toward the form-dominated state. Floods have been smaller in recent years, due to either climatic effects or morphologic feedback, or a combination of the two. The channel is shrinking in width and meandering only slowly, continuing to provide new ground for colonization.

VEGETATION DESCRIPTION

The vegetation of the middle Fremont, as recorded in 1982 at the mile-post 111 traverse (fig. 10), is typical of the river between Caineville and Hanksville. Colonization by reed mats and seedlings of coyote willow and tamarisk begins on the active shelf (AS in fig. 10). Cottonwood probably appears here as well during favorable years. A row of cottonwood saplings to five meters in height occupies the proximal flood bar (FB) with some Russian olive, tamarisk, coyote willow, and rabbitbrush, with ground cover ranging from 30 to 50%. The cottonwood saplings belong to a single cohort which is dated to the early 1970's, and is probably a response to the late spring flood of 1973 (Everitt, 1995). The distal flood bar is occupied by tamarisk and rabbitbrush, with ground cover estimated at 60%. In the inter-

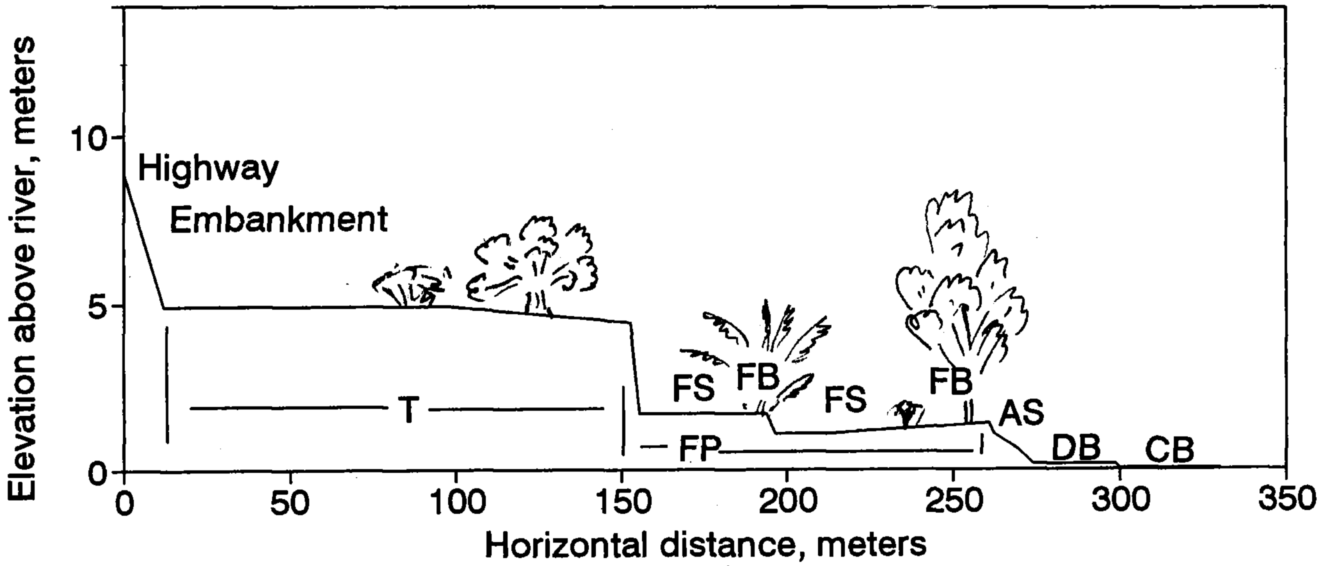

Figure 10. Pace and hand-level traverse of Fremont River Valley, running S 16 W from milepost 111, State Highway 24. The physiographic subdivisions of the valley floor are labeled with binomial initials: CB, channel bed; DB, depositional bar; AS, active channel shelf; FP, active flood plain; FB, flood bar; FS, floodplain swale; T, terrace—abandoned floodplain (from Everitt, 1995, Figure 4).

vening swales (FS) are rabbitbrush, tamarisk, four-wing saltbush, and Torrey seepweed to a lower density (10 to 20%). The dense fringe of tamarisk at the toe of the terrace is a widespread feature of the central Fremont, and indicates that tamarisk was the primary perennial pioneer species at the time the active channel margin began to retreat from the foot of the terrace.

The terrace (T) is occupied by four-wing saltbush and greasewood, with some old cottonwoods, many dead or dying. The absence of tamarisk shows that the terrace predates the introduction of tamarisk into the Fremont drainage.

CONCLUSION

The simple pioneer-dominated plant community of the Fremont River flood plain records a changing mix of species in response to changing habitat and the introduction of new species. Recorded in the transect at milepost 111 is the introduction of tamarisk (probably about 1940) and its subsequent decline; the resurgence of cottonwood in the 1970's, and a continuing gradual increase in Russian olive (Everitt, 1995).

Gravel Deposits North of Mount Ellen, Henry Mountains, Utah—Part 5

ANDREW E. GODFREY

INTRODUCTION

The piedmont north and northeast of Mount Ellen, northernmost of the Henry Mountains, is marked by fan-shaped gravel deposits of three streams. These deposits are the gravel-capped pediments of Gilbert (1880, p. 120–129), and Hunt, et.al. (1953, p. 189–195). From east to west the streams are Bull, Birch, and Nazer Creeks. A program of detailed mapping was undertaken to determine the history, mode of deposition, and controlling factors of these gravel deposits (Godfrey, 1969). This report presents a brief overview of the findings related to Bull Creek.

FINDINGS

A band of hummocky, boulder-strewn deposits separates Mt. Ellen's slopes from smooth-surfaced gravel deposits farther out. This band, containing boulders that range up to house size, is considered to be deposits of an Early Pleistocene debris avalanche (Godfrey, 1980).

Mapping of the smooth-surfaced gravel deposits showed they are a composite of discrete linear deposits extending from the mountain front to the Fremont-Dirty Devil river system. Figure 11 shows the directions of several paleocourses of Bull Creek. Additional, minor routes are not shown. For Bull Creek there were at least 13 distinct gravel deposits representing different stream courses.

This investigation indicated that, in the piedmont north of the Henry Mountains, the development of a gravel bench is a repetitive process. It begins with gully erosion of some older piedmont landform. However, the critical factor is the gradient of streams tributary to main streams originating in the mountains. Unlike the more common case, where tributaries have steeper gradients than the main stem, tributary desert washes not draining igneous rocks have flatter gradients. These washes are eroding and transporting only fine-grained erosion products of sedimentary units exposed on the piedmont rather than the coarse products of the igneous mountain mass. This difference in gradients results in each tributary being at a lower elevation than the adjacent main stem at any point upstream from the junction.

Erosion of drainage divides, random lateral migration of mountain streams across their flood plains, and overflow of a divide during a flood, can lead to the capture of the headwaters of a main stem stream by a nearby desert wash. With the diversion of the gravel-transporting stream, the valley of the desert wash changes from a locus of erosion to one of deposition. This change results in the steepening of the

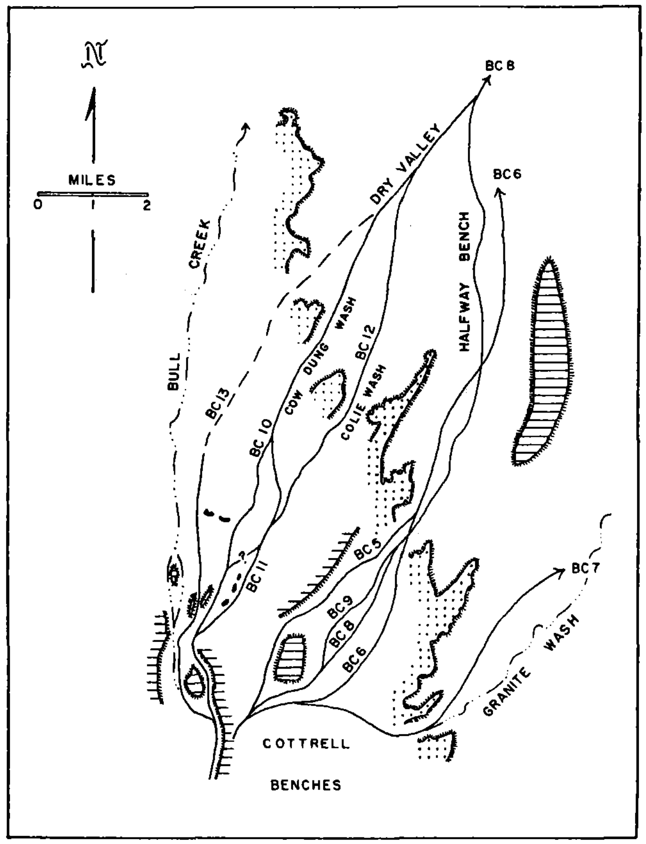

Figure 11. Sequential changes of ancestral Bull Creek interpreted from gravel deposits on the Cottrell and Fairview Benches. Higher numbers are younger deposits. Hatchers represent escarpments, stiples are on the dip slope of the Summerville Escarpment, horizontal rulings represent higher-standing gravel deposits, and black areas represent sandstone hills at or just above the level of the gravels. In general, the sequence shows a progressive headward capture of the main stream.

wash's gradient so the wash can transport the coarse gravel. Accompanying this steepening of gradient is a regrading of the point of capture into a smooth profile.

During burial of the former desert wash's valley, its floor can be smoothed by lateral planation. However, the linear nature of the mapped gravels indicates that this lateral planation is restricted to the already existing valley. There is little widening by the gravel-carrying streams, perhaps due to the steepness of the slopes in this area. Braided streams have distributed gravels over flood plains whose limits have been predetermined by the width of the pre-existing valley.

CONCLUSIONS

Detailed mapping of Bull Creek's gravel benches north of Mount Ellen showed that the apparent fan-shaped, gravel-capped pediments are a composite of several linear deposits, each representing an identifiable stream course at progressively lower levels. They fit Robert Oak's classification of a "shoestring" pediment (Oaks, personal communication). This is because the gravels were deposited in pre-existing valleys cut by desert washes. Lateral planation can occur within a valley, but widens it only slightly in areas of steep slopes.

The processes that form these gravel benches are not climatically controlled. There is not one set of conditions that causes erosion and another set that favors deposition. Both erosion and deposition can occur simultaneously. Desert washes with lower gradients erode valleys in the piedmont that are at lower elevations upstream from their confluences than the aggradational, higher-gradient, gravel-bearing main streams flowing out of the mountains (Rich, 1935). Capture occurs randomly when the main stream migrates to the edge of its valley where its interfluve has been eroded away.

Relative relief between gravel benches is not necessarily an indicator of the time between the deposition of the benches. Instead, distance between capture point and downstream confluence, and the resistance of the rocks that a desert wash erodes through, are significant controls of relief.

Monitoring flash floods in the Upper Blue Hills Badlands, Southern Utah—Part 6

GREGORY S. DICK
ROBERT S. ANDERSON
DANIEL E. SAMPSON
Department of Earth Sciences and Institute of Tectonics, University of California, Santa Cruz, California 95064

Why study badlands, or flash floods, or flash floods in badlands?

Badlands are intriguing for their unique and often desolate appearance and apparently rapid rates of change. These barren landscapes develop through intense fluvial dissection that produces steep hillslopes and high local relief (Bryan and Yair, 1982; Howard, 1994), and are most often found on easily eroded, "soft" bedrock (e.g., shales) in arid to semi-arid environments. Spot hillslope erosion rates in badlands on the order of mm/yr are among the highest measured in any landscape (Schumm, 1956; Schumm, 1964; Campbell, 1982). The short time scales during which badlands develop and their manageable spatial scales (e.g., area, relief) provide us with a geomorphic microcosm in which to study fluvially controlled landform evolution.

Because hillslopes erode quickly, maintenance of the rugged topography in the Upper Blue Hills (Blue Hills) requires high channel incision rates. The typical assumption is that the regolith and bedrock common in badlands are easily erodable, coupled with nearly impermeable regolith, leading to high runoff/rainfall ratios. High runoff appears to be needed to cause high rates of incision. While these shales are visibly quite friable, much existing work challenges the notion that badlands surfaces are simply impermeable "parking lots" (Schumm and Lusby, 1963; Lusby, 1979; Yair et al., 1980; Bryan et al., 1984). The heavily cracked and piped regolith in badlands is often highly permeable, with maximum potential infiltration rates on par with maximum rainfall intensities (~50–100 mm/hr). Yair et al., (1980) , comparing experimental infiltration rates to rainfall records, conclude that surface flow in the Zin badlands of Israel is exceedingly rare under the present climate, and is produced only during extreme rainfall events. Apparently, only a few rainfall events produce surface flow in these landscapes under present climate conditions.

The combination of rapid channel erosion with apparently rare flow events poses an interesting problem: when and how are these channels eroded? Are rare, large-magnitude rainfall events the only way, or can less frequent events accomplish much geomorphic work? To decipher this, we need documentation of the frequency and erosive power of flows in these channels, but little flow information is available for such small catchments. In fact, there are few measurements of flash floods in general, as they are rare and difficult to gauge accurately. However, the limited observations suggest they are quite different from that of perennial flows. They are typically highly turbulent, and carry extremely high suspended sediment loads relative to perennial flows of similar size (Reid and Frostick, 1987). Typical flash floods initiate with the passage of a small, steep-faced bore front, immediately followed by some flow recession. Thereafter, the hydrograph gradually rises to peak depth. The time to peak discharge is short, and decreases with increasing drainage area as the hydrograph front steepens downstream. Recession is typically rapid. Excellent discussions of flash floods are available (Hassan, 1990; Leopold and Miller, 1956; Reid and Frostick, 1987; Renard and Keppel, 1966; and Schick, 1988).

To learn how often erosive flows occur in the Blue Hills, we began actively (and accurately) monitoring channel flow and rainfall in the Upper Blue Hills in early summer 1994. Our aim is to address the following questions: (1) what is the hydraulic nature of the ephemeral flows in these channels, and what produces the observed characteristics?; and (2) what controls the frequency and magnitude of geomorphically significant flow events?

The Blue Hills Flash-Flood-Monitoring Project

The Upper Blue Hills badlands

The Upper Blue Hills badlands extend from the Henry Mountains to the south (Mt. Ellen, at 3510 m, is the highest peak in the Henry Mountains), to North Caineville Mesa and Factory Butte, just to the north and northeast. Channels drain to the Fremont River, a tributary to the Colorado River. The blue-gray marine shales in the Blue Hills belong to the Blue Gate Member of the Cretaceous Mancos Shale, which floors roughly one-sixth of the upper Colorado River basin. The climate is arid: Hanksville, ~25 km east, receives an average of 12±4 cm annual rainfall (period 1947–1992). Local convective thunderstorms occur during the summer, when the warm continental interior draws monsoonal winds off the Gulf of California. Frontal storms deliver low-intensity rainfall (and some snow in winter) during the remainder of the year.

The Blue Hills provide a stunning visual example of the intimate linkage between hillslopes and channels in fluvial landscapes. Drainage densities in the instrumented basin are high, exceeding 60 km/km^2. Channels along the instrumented reach have slopes >0.01, with frequent knickpoints up to ~1 m in relief in bedrock and alluvium, and alternate between short bedrock reaches and reaches covered with a thin (<0.5 m) alluvial mantle. The erosion of the channels is accomplished through: (1) direct, subaerial (perhaps salt expansion) weathering of the bedrock channel floor, with weathering products transported in flows; (2) disaggregation of the rock by water (drop a piece of the Mancos Fm in your water bottle!); (3) headward propagation of knickpoints throughout the badlands; and (4) some direct "plucking" of blocks and rock fragments from the bed which are likely later weathered or disassociated by water. The hills are evolving through a combination of diffusive rain-splash erosion along the ridge lines (note convexity and "smooth" look) where slope is gentle, and shallow (~few cm's) landsliding on steeper hillslopes. The transition to landslide-dominated erosion is quite visible on the hillslopes, and typically occurs at slope angles of 35°–40°. Hillslopes are rarely steeper than this, except where actively undercut by channel meanders. Steep hillslopes are maintained by incision of the adjacent channels. Such landslides transport a substantial quantity of material to the channels, where it is later transported by channeled flows and thereby helps generate the high sediment concentrations in flows from the Blue Hills. Erosion by overland flow (i.e., sheetflow) appears to be minimal, although there is evidence of regolith stripping by small mudflows in the rills.

The Blue Hills are evolving through headward channel incision likely initiated by rapid post-glacial incision of the Fremont River (Howard, 1970). This incision is recorded by the terraces now visible along the Fremont. The isolated, relatively smooth surfaces that cap the badlands here are inferred to be paleovalleys mantled with debris-flow material from the adjacent buttes; the debris-flows are perhaps most active during pluvial (glacial) episodes. These surfaces appear to grade to a Fremont River terrace, although correlating these remnant surfaces is tricky. Cosmogenic radionuclide dating of the large remnant along the western edge of the monitored basin yields ages of ~18 kyr (unpubl. data, J.L. Repka). This age ties debris-flow deposition on this surface to the last glacial maximum. If this date records the approximate time of abandonment, the current relief of the monitored catchment implies average post-pluvial channel erosion rates up to ~2 mm/yr. This scenario of badland development through post-pluvial incision of a trunk stream is similar for badland development elsewhere in western North America (e.g., Bryan et al., 1987).

Hydrograph measurement technique

Because flash flows are turbulent, sediment-laden, rare, and rapidly varying, and because we needed a gauging technique that could operate without frequent maintenance, we developed an acoustic depth monitoring system, dubbed the EchoRanger. The acoustic sensors, which are based on Polaroid autofocus camera electronics, are hung below PVC supports, and "look" down on the channel floor. The sensors are connected and controlled by a Campbell Scientific CR10 datalogger located in watertight control boxes adjacent to the channel. These sensors obtain distance measurements to a reflector by measuring the travel time of an emitted pulse of sound, and can obtain distances as frequently as 8 Hz;. Here, we operated them at 1 Hz. The recorded distance between the sensor and a reflective surface (either water or channel bottom) is converted to a flow depth, from field calibrations, after correcting for temperature.

We deployed four stations (A–D), each with two acoustic transducers, along the same channel, and one recording, tipping-bucket rain gauge at station B (fig. 12). Gauged basin sizes are from 0.88 km^2 to 1.03 km^2 (fig. 12). Rainfall was totaled at 1 minute intervals, and ambient temperature was recorded whenever depth readings were saved.

Recorded hydrographs

From summer 1994 to summer 1996, we have evidence for 11 flows in the monitored catchment. Seven of these events were relatively small (peaks <0.15 m^3/s); only four flows exceeded 0.5 m^3/s. We focus here on the two hydrographs discussed in Dick et al., (1997).

Event A: September 20, 1994

On September 20, 1994, we witnessed a rainfall event that produced a small flow. The rain gauge recorded 4.8 mm during a period of 8 min, with intensities ranging from 15 to 76 mm/hr. Rills on hillslopes contained visible runoff within several minutes after rainfall began, especially following the highest rainfall intensity. The heavily cracked

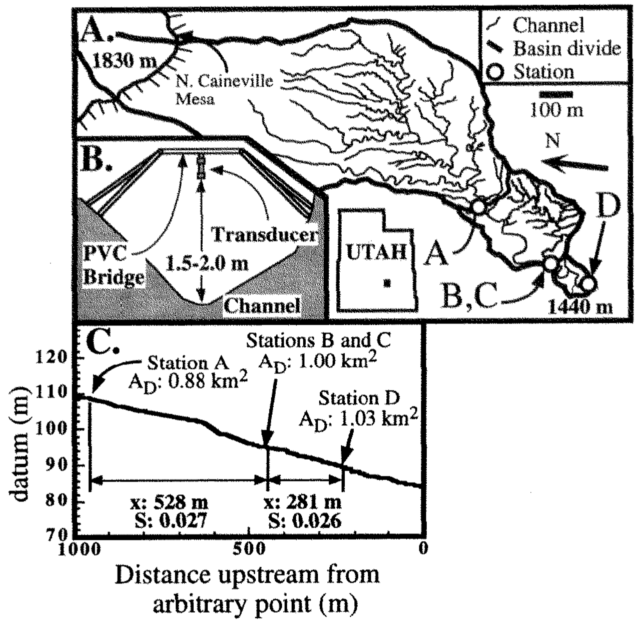

Figure 12. A: Drainage network and location of gauging stations location. B: Schematic of acoustic-sensor installation. C: Profile of main channel through monitored area, with total drainage area (A_D) above each station, and horizontal distance (x) and average slope (s) between each station.

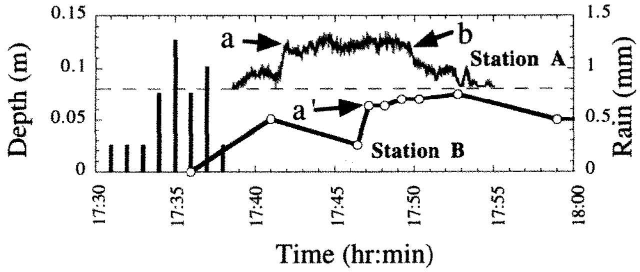

Figure 13. Event A hyetograph (bars) and hydrographs for stations A and B. Black line is 3 s running average of d *measured every 1 s; gray line shows 1 s data. Scatter in the 1 s data is indicative of measurement error. Dashed line is recording threshold (~8 cm). Hand-held measurements at station B were made at times shown. We collected during any notable changes in flow, and the hydrograph between gauging points did not depart significantly (±1 cm) from the line connecting the points. Average translation velocity for rapid rise in flow level, labeled a-a′, was 1.8 m/s over 0.5 km reach between stations A and B. Note several distinct flow peaks of station A hydrograph, and rapid depth changes at a and b that are large relative to total depth.*

regolith did not seal during the rainfall, and we did not observe concentrated surface flow on undisturbed regolith. Depth of regolith wetting was up to a few centimeters. Surface failures ~5 cm deep occurring during the storm revealed a dry bedrock surface.

We measured flow depth and surface velocity manually at station B (fig. 13). Flow began ~5 min into the rainfall event, and gradually increased to several centimeters depth by rainfall completion. Two bores of several centimeters height passed ~9 and ~16 min after rainfall began. Surface velocity measurements ranged from 0.7 m/s (depth = 2.5 cm) to 1.9 m/s (depth = 7.0 cm). Standing waves were observed at depths ≥ 2.5 cm, evidence of near critical (Fr = ~1) flow conditions (Knighton, 1984). Flow Reynolds numbers were ≤ 41 000. Measured surface velocities yielded n values from 0.012 (depth = 7.5 cm) to 0.022 (depth = 2.5 cm).

The station A acoustic system recorded flow above the ~8 cm threshold (fig. 13). Depth at the remaining stations was below the recording thresholds (<10 cm). The hydrograph is complex: there were numerous rapid changes in depth that were large relative to the total depth. The average translation velocity of the rapid rise of flow level (a at A, a′ at B, fig. 13) was ~1.8 m/s. The estimated runoff coefficient (total runoff/total rainfall) was ~0.01.

Event B: September 29–30, 1994

On September 29–30, 1994, a rainfall event lasting 30 min and totaling 5.3 mm produced the deepest recorded flow (fig. 14). Rainfall intensities were low (<30 mm/hr). However, 3.0 mm of rain had fallen during the preceding 12 hr. Three stations recorded the resulting hydrograph (fig. 14).

At each station, depth increased rapidly, rising from below the recording threshold to ~15–20 cm in <~5 min (fig. 14). This initial front advanced with an average velocity of 2.0 m/s from station A to B and 1.5 m/s from station B to D, and retained a height of ~20 cm. The rise time to the initial flow peak (a-a″, fig. 14) shortened from ~5 min at station A to ~3 min at station D. The initial peak was followed by recession of several centimeters, and later by two primary flow peaks (b and c, fig. 14) presumably associated with individual rainfall maxima within the storm. Features identifiable in each hydrograph (a, b, and c, fig. 14) traveled with velocities of 1.2 to 2.2 m/s, increasing with flow depth. The time lag between the start of flow recording and peak flow was ~15 min at each station. Runoff coefficients were ≥ ~0.08.

Controls on hydrograph shape and total runoff

Events A and B had different hydrograph characteristics. We suggest that this may reflect differences in rainfall delivery. In the event A hydrograph, produced by an intense thunderstorm (fig. 13), large depth changes (relative to total

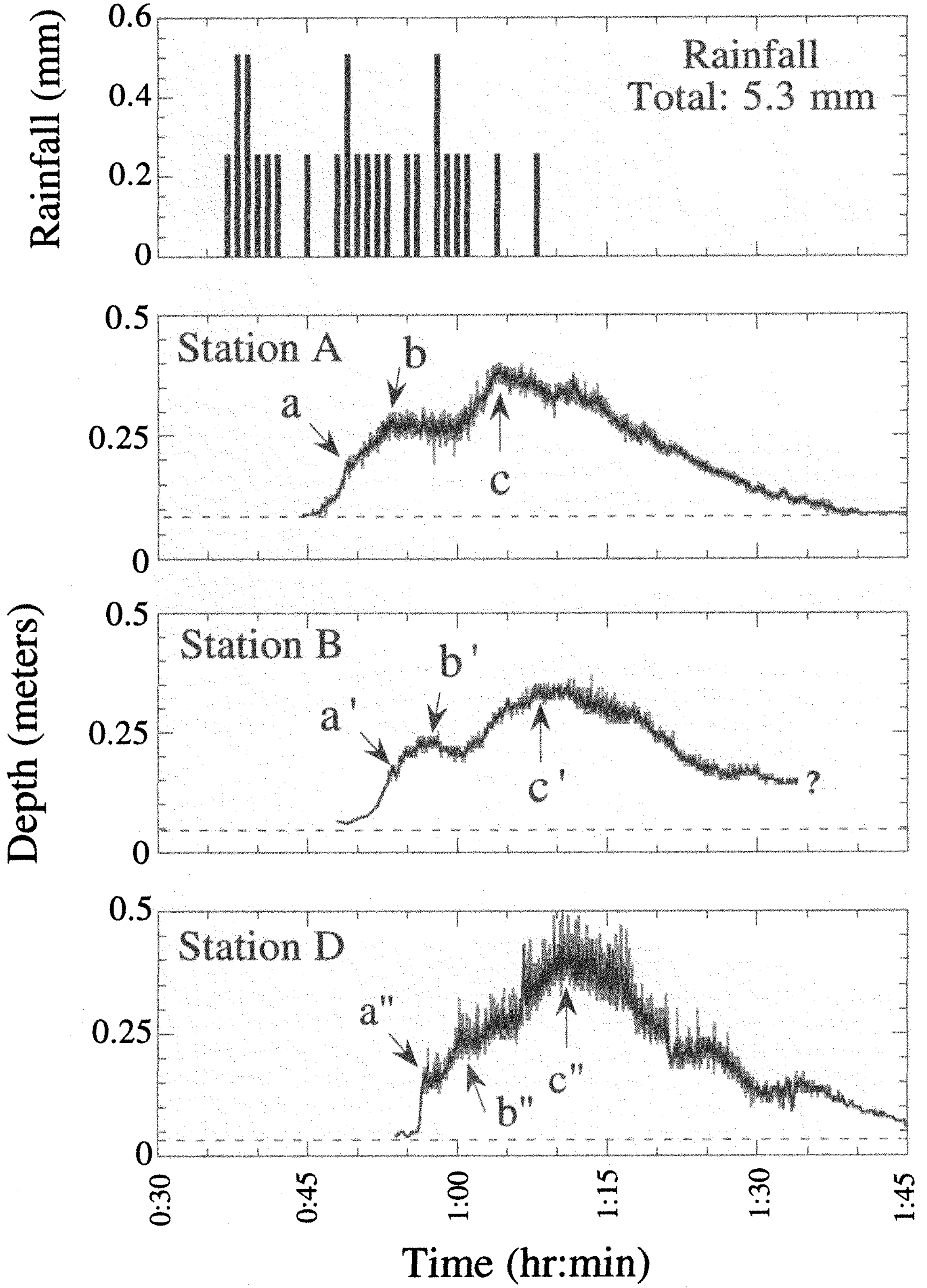

Figure 14. Event B hyetograph (top graph) and hydrographs for stations A, B, and D. Dashed lines as in Figure 3. Large scatter in station D data arises from false triggering of sensor by splash. Note reduced rise time to initial hydrograph peak (a-a′-a″) and overriding of b-b′-b″ by peak c-c′-c″ during hydrograph translation downchannel. Features a, b, and c are selected where hydrograph curvature is high. Average velocity (m/s) of hydrograph features: a-a′ = 2.0, b-b′ = 1.9, c-c′ = 2.2, a′-a″ = 1.5, b′-b″ = 1.2, and c′-c″ = 1.8.

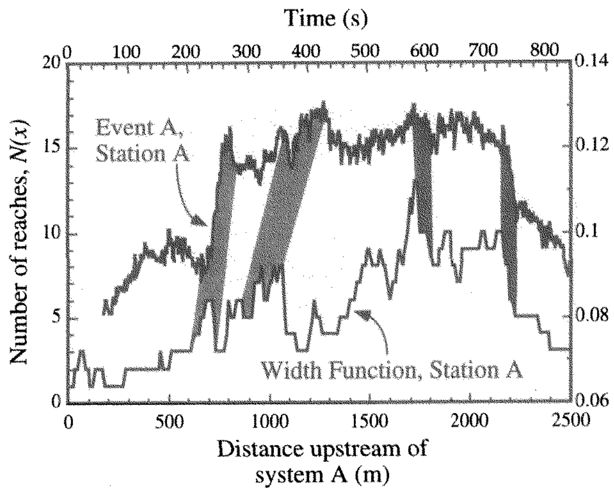

Figure 15. Comparison of event A, station A hydrograph (d *vs. time) and the network width function (see text) for basin above station A. Gray boxes highlight similarities between the two curves.*

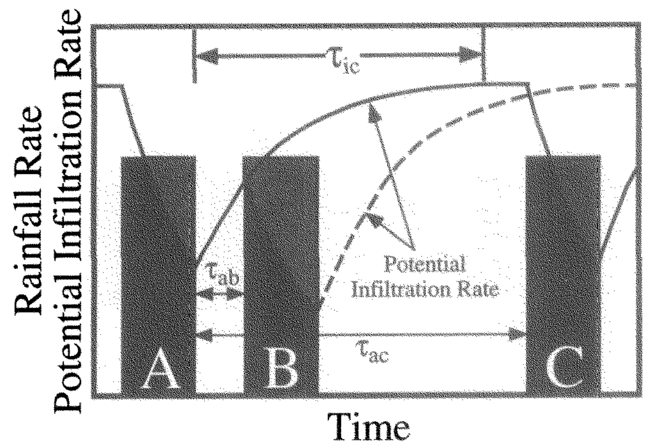

Figure 16. Schematic illustration of important antecedent-moisture time scales using three simplistic boxcar-shaped "storms" of equal intensity and duration (A, B, and C), shown as rainfall-intensity histories. Rainfall event A decreases potential regolith infiltration rate (solid line), so that eventually the constant rainfall intensity exceeds this rate, producing runoff (light gray area of rainfall boxes). Infiltration capacity begins to recover following completion of storm A. Full infiltration capacity recovers fully in time tic. Time between storms A and C, τ_{ac}, is long enough ($\tau_{ic}/\tau_{ac} \leq 1$) for infiltration capacity to have fully recovered. Time between storms A and B, τ_{ab}, is short ($\tau_{ic}/\tau_{ab} > 1$); the infiltration capacity has not recovered from previous wetting. Further decrease in infiltration rate (dashed line) during storm B allows production of much more runoff than equal-sized storms A and C.

depth) are frequent and occasionally rapid (a and b, fig. 13). Similar rapid depth fluctuations observed in other flash floods were suggested to be either "momentum waves" (Leopold and Miller, 1956), or an expression of the channel-network shape (e.g., Renard and Keppel, 1966). We compare the event A hydrograph to the graphical network width function, which is the sum of channel segments as function of distance above a point in the channel network (fig. 15; see Mesa and Mifflin, 1986, and Dick et al., 1997, for details). The event A hydrograph and the network width function are similar (fig. 15), which suggests that the hydrograph shape could reflect the network geometry. The only other recorded hydrograph produced by a high-intensity storm also looks similar to the width function, despite differences in the hyetograph (Dick, 1995). In contrast, the event B hydrograph is much smoother, lacks obvious features reflecting network shape, and is broadly similar in shape to the rainfall hyetograph. We hypothesize hydrograph shape is controlled by the network geometry when flow is produced by high-intensity storms that are short relative to the rise time of the hydrograph (e.g., event A). In such cases, overland and shallow subsurface flow produce rapid runoff; tributary flows are short-lived, and contribute peaks to the trunk channel that are preserved in the outflow hydrograph. For storms of similar size but longer duration (i.e., event B), tributary hydrographs rise more slowly, with smaller peaks that are not clearly preserved in the outflow hydrograph. We continue to collect data here to test these hypotheses.

A critical factor in runoff generation here is antecedent moisture. The difference in the two flow events we describe here is a good model. The events had comparable total rainfall (4.8 mm in event A and 5.3 mm in event B), but, counterintuitively, the storm with lower intensity produced flow with maximum discharge and total energy expenditure an order of magnitude greater than event A, produced by a more intense storm (up to 76 mm/hr). The outstanding difference between the two events is the antecedent moisture condition: whereas no rain fell in the 9 days prior to event A, 3.0 mm fell intermittently during the 12 hr preceding event B. The reduced potential regolith infiltration rate allowed significant runoff production ($\geq$ 8% total rainfall vs. ~1% in event A). In fact, of 33 rainfall events exceeding 0.5 mm total rainfall recorded in 1994 and 1995, only three produced flows with maximum discharges >0.5 m^3/s. These three rainfall events, although not remarkable in total rainfall (1.2, 5.3, and 6.6 mm), were preceded by >3.0 mm rainfall during the previous 24 hr. The remaining 30 rainfall events occurred when rainfall was $\leq$ 1.8 mm during the preceding 24 hr, and produced little or no flow.

For antecedent moisture to be important, storms must occur within some time, τ_{ic}, after a previous wetting event (fig. 16). This time scale reflects how quickly infiltration capacity is recovered through drying, which depends upon regolith properties and weather (e.g., temperature, wind). We estimate τ_{ic} to be roughly 24 hr in the Upper Blue Hills. Because of this recovery time, we must know the full probability distribution of spacing between rain events to estimate flow frequency. The average time between storms (e.g., Schumm and Lusby, 1963) is not sufficient, because storms are not evenly spaced. For instance, the total energy expenditure suggests that event B was geomorphically significant (Costa and O'Connor, 1995). The total rainfall for event B has a return period of ~1 yr.. However, geomorphically important event B-type channel flows may occur at a quite different frequency dependent on storm-sequencing rather than rainfall recurrence interval.

Dating the Fremont River Terraces—Part 7

JAMES L. REPKA
ROBERT S. ANDERSON
GREG S. DICK
Department of Earth Sciences and Institute for Tectonics, University of California, Santa Cruz, California 95064

ROBERT C. FINKEL
Geosciences and Environmental Technology Division and Center for Accelerator Mass Spectrometry, Lawrence Livermore National Laboratory, Livermore, California 94550

ABSTRACT

In many parts of the world, sequences of terraces that flank river drainages mark periods of stasis in the downcutting history of the river. Absolute dating of these terraces, in addition to yielding long-term incision rates, can clarify the role of climate in controlling river-drainage evolution and can establish the rates of pedogenic processes. Surface exposure dating using cosmogenic ^{10}Be and ^{26}Al would seem to be an ideal way to date such surfaces. However, the surfaces are composed of individual clasts, each with its own complex history of exposure and burial. Because the exposure age of a clast may be different than the exposure age of the surface, the stochastic nature of nuclide production in the clasts, both during their exhumation and transport to fluvial terraces as well as during post-depositional stirring, can result in neighboring clasts containing grossly different nuclide concentrations. We describe here a strategy for dealing with the problem of the stochastic nature of inheritance. First we study samples amalgamated from individual clasts in order to average the widely different exposure histories of each. Second, we measure samples from depth profiles to estimate the actual level of inheritance and to check for the possible importance of stirring.

The results of applying this technique to terraces along the Fremont River in southern Utah demonstrate that single clast ages are indeed more widely scattered than those of amalgamated samples and that samples amalgamated from 30 clasts represent the mean concentration quite well. Depth profiles consisting of several amalgamated samples show an exponential decline in concentration attributable to post-depositional nuclide production, and argue strongly against relative displacements of the clasts on these horizontal surfaces subsequent to deposition. Using the production rates of Nishiizumi et al., (1996) as adjusted for geographic latitude and for reassessment of the deglaciation age (Clark et al., 1995), our technique yields ^{10}Be age estimates of 60 ± 9, 102 ± 16 and 151 ± 24 ka for the three most extensive terraces, corresponding to isotope stages 4, 5d and 6. Isotope stage 2 appears to be represented here by either a small group of isolated narrow surfaces or by the current flood plain of the Fremont River. These dates support a conceptual model in which the terraces formed when there was a strong glacial source of sediment within the headwaters, and were abandoned when the sediment source shut off. The mean inheritance is remarkably constant from terrace to terrace. Failure to correct for inheritance would yield dates several tens of thousands of years too old. Inheritance likely reflects primarily the mean exhumation rates in the headwaters, of order 30 m/Ma.

The channels of the Blue Hills badlands have as their base level the channel of the Fremont River (fig. 17). The numerous extensive terraces of the Fremont River attest to the lowering of this boundary condition through time. To begin to assess the history of this downcutting, and hence the history of the baselevel forcing that was experienced by the adjacent badlands, we set out to establish the ages of these Fremont terraces. While these surfaces were mapped in detail by Howard (1970) in his thesis work, no absolute ages exist. As the headwaters of the Fremont have experienced a.

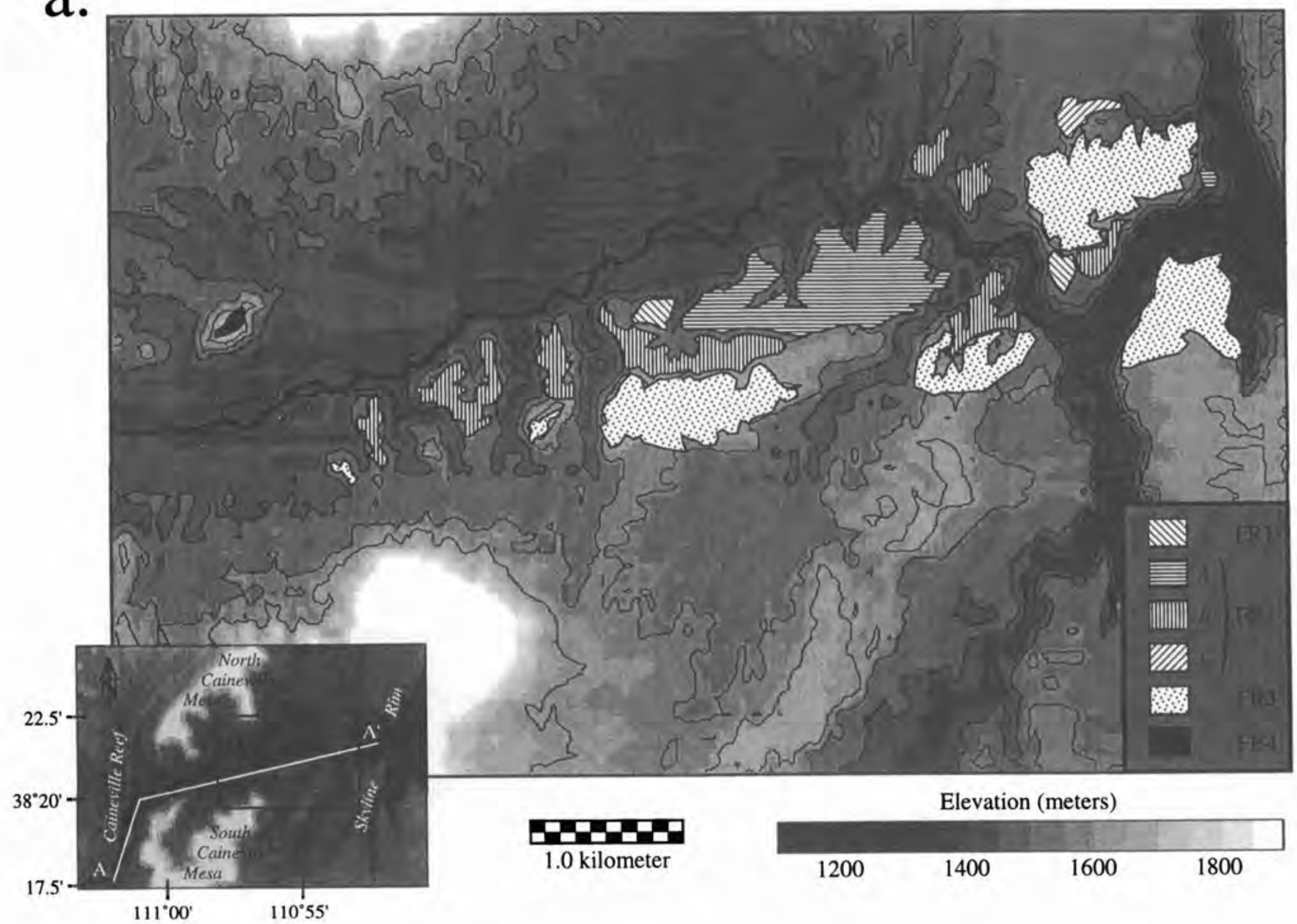

b.

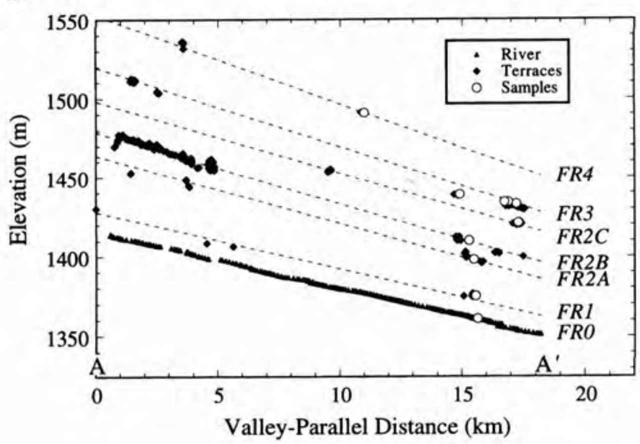

*Figure 17. (**a**) Detailed topography adjacent to the Fremont River as it passes eastward through the gap between North and South Caineville Mesas. The sampled terraces are depicted. Note the isolated scraps of FR1 and FR4 surfaces, and the extensive preservation of FR2 and FR3 surfaces. (**b**) Valley-parallel longitudinal section of the terraces (diamonds) in the study area (A-A′ from the inset map in Figure 17a), showing elevations relative to the modern Fremont River floodplain (triangles). Sampled sites are shown as open circles.*

occasional glaciation (Flint and Denny, 1956), the sediment- and water-discharge histories from the headwaters should have seen large swings that result in downstream propagation of waves of aggradation followed by incision and abandonment of outwash terraces (e.g., Bull, 1991). The glacial deposits in the headwaters are not well dated. In addition, correlation to other glacial sequences within the western U.S., such as those in Wind River system (Howard, 1986), implicitly assumes the synchroneity of the responses to regional climate change. Absolute dates of these, and of other sequences of glacial outwash terraces in the western U.S., would allow testing of the conceptual model for the formation of such terraces, and would allow assessment of the degree to which these isolated alpine glacial systems responded in phase with one another and with continental ice sheets through the late Pleistocene glacial ages.

We have employed ^{10}Be and ^{26}Al, cosmogenic radionuclides produced *in situ* (see, for instance, Bierman, 1994; Cerling and Craig, 1994; Finkel and Suter, 1993; Lal, 1991; Nishiizumi et al., 1993) to date the most extensive of the surfaces exposed along the Fremont River as it passes between the Caineville Mesas (fig. 17). Cosmogenic radionuclides are produced by the energetic impacts of secondary particles produced by cosmic rays with near-surface materials, ^{10}Be largely from impacts with oxygen, and ^{26}Al largely from impacts with silicon. Quartz is an ideal target mineral because it contains two of the primary target elements and because its resistance to weathering allows it to retain the cosmogenic radionuclides. The half-lives of ^{10}Be (1.5 Ma) and ^{26}Al (0.7 Ma) make them appropriate candidates for dating surfaces throughout the Quaternary.

There is a down side, however. Because cosmogenic radionuclides are produced whenever a rock is within roughly 2 meters of the earth's surface, the cosmogenic radionuclide clock starts to tick well before a clast is embedded within its present deposit. It will have inherited radionuclides both during exhumation from a hillslope within the headwaters, and as it travels through the fluvial system, stopping here and there in the flood plain. Each clast will have its own individual history, reflecting the particular route it took to get to the final terrace site. All clasts will arrive with at least a few ticks on the cosmogenic clock. The trick is to see through this inheritance to extract the age of the surface. We have outlined a technique designed to do just this (Anderson et al., 1996): We show here our latest results, applied to the Fremont River terraces.

One possibility would be to analyze many clasts from the surface and to take the clast with the lowest concentration of radionuclides as having been emplaced with minimal inheritance. Its concentration could then be inverted for the time since emplacement on the surface, and knowing the production rate and the decay constant, one could back out the age of the surface. (Crudely, ignoring decay, the effective age is $T=N/P_0$, where N is the measured concentration of cosmogenic radionuclides, and P_0 is the surface production rate). Unfortunately, cosmogenic radionuclide analysis is both expensive and time consuming, making it difficult to analyze a sufficient number of individual clasts to map out the distribution of inheritance. Our initial experiments with single clasts demonstrate that the concentrations and hence effective ages are indeed widely spread (Repka et al., in press).

Our technique is based upon the following conceptual model of the geomorphic system (fig. 18): The depositional system was that of a braided outwash plain, and the deposit at the site we ultimately sample accumulated rapidly over time scales that are very short (probably 100s of years at the most) compared to the age of the terrace. Inheritance varies randomly from clast to clast because the exhumation rate within the basin is nonuniform, and because the transit times and burial depths during transit within the fluvial system vary. Abandonment of the terrace occurred as the river incised into the weak Mancos shale bedrock, presumably when sediment supply in the headwaters declined as the glacial system collapsed. Subsequent to abandonment, the surface of the terrace slowly agraded with eolian dust to produce a loess blanket 10–20 cm thick. A desert pavement developed in which a monolayer of clasts remained atop the dust mantle (Wells et al., 1995). A soil developed in which gypsum and carbonate cements dominate, but actual turbation of the subsurface clasts was minimal. The distribution of lithologies of the clasts on the surface evolved as those most susceptible to weathering disintegrated. Locally derived sandstones and shales disintegrated rapidly, while quartzites derived from the middle Mesozoic outcrops 20–30 km upstream prove to be the most resistant (Billingsly et al., 1987).

Given this picture, which is developed from field observations of the Fremont terrace sequence, we can assume that the terrace deposit was rapidly emplaced and the depth history of any individual clast within the deposit can be well constrained, both by its present depth and the thickness of the eolian silt. We collect a series of samples from several discrete depths within the terrace gravel deposit, each sample consisting of several dozen quartzite clasts. Back in the lab we construct an amalgamated sample from each horizon, taking mass aliquots from each clast so that no single large clast dominates the signal at a particular horizon. If we have taken enough clasts, the cosmogenic radionuclide concentration of this sample therefore approximates the mean concentration of clasts at that depth. At the time of deposition the profile of mean concentration versus depth should be uniform and reflect the mean cos-

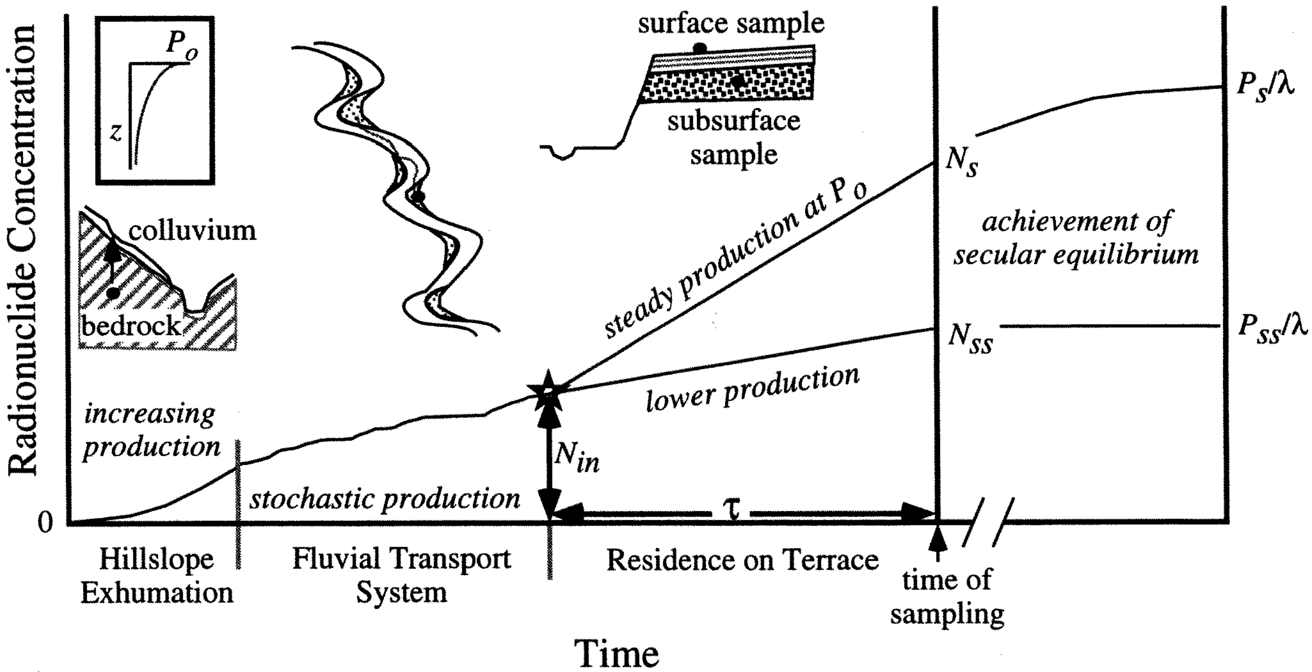

Figure 18. History of the cosmogenic radionuclide concentration of a hypothetical clast, following its transport history in hillslope and fluvial systems, and in its subsequent residence at its present site. Production rate is dictated by depth beneath the local surface, z, which falls off exponentially with depth (see inset). Exhumation on hillslope results in monotonic increase in concentration. Production history is stochastic within the fluvial system, when a clast travels between point bars and then is buried to differing depths. Evolution of concentration on final terrace site is shown for two possible burial depths, one on surface, other in subsurface. One scenario for surface clast is that it remains on the silt surface, in which case it always experiences the surface production rate, P_0, *and attains sampled concentration of* N_s. *The subsurface clast within underlying gravels (stippled) will undergo a lower production rate, and is sampled with concentration* N_{ss}. *Clasts on terraces much older than nuclide half lives attain secular equilibrium, with labeled concentrations. Amalgamated samples consisting of numerous clasts allow back-calculation of terrace age, τ, and of the mean inherited radionuclide concentration,* N_{in}.

mogenic radionuclide inheritance of the clasts within the geomorphic delivery system. Because the production rate falls off exponentially with depth beneath the surface, and because the clasts have not moved relative to one another in the subsurface, we expect that the post-depositional cosmogenic radionuclide profile should look exponential. The sum of inherited cosmogenic radionuclides and post-depositional cosmogenic radionuclides should therefore produce an exponential profile that is simply shifted or offset.

The results on the Fremont terraces support the validity of our technique (fig. 19). Where we have generated full cosmogenic radionuclide profiles, these show the expected shifted exponential form, from which we can extract both the inheritance (from the shift) and the age of the surface (from the exponential). This broadly supports the series of assumptions we have made in the above conceptual model of the origin and evolution of these surfaces. The inheritance is large. Clasts arrive on the final terrace surface with effective ages up to several tens of thousands of years. This implies that, without taking inheritance into account, age estimates based upon single clasts would be far too old. Using the latest published production rates for ^{10}Be (Nishiizumi et al., 1996), our technique yields estimates of the ages of the most prominent of the terraces to be 60±9 ka, 102±16 ka and 151±24 ka, which correspond to benthonic-plankton isotope stages 4, 5d and early stage 6 (fig. 20). The ^{26}Al results yield similar age estimates.

We note that at this location there is no well expressed terrace that corresponds to isotope stage 2 (Last Glacial Maximum). There are two surfaces here that may represent isotope stage 2: One is a narrow, intermittent terrace 10 meters above the river (FR 1); our cosmogenic radionuclide results from this surface are inconsistent with those on other surfaces (fig. 19). This difference may reflect poor access to the subsurface in our sampling and/or a burial of the surface by colluvium from a higher terrace. It is also possible that the stage 2 glaciation is represented here by the current flood plain (FR0). In either case, the minor, narrow exposures

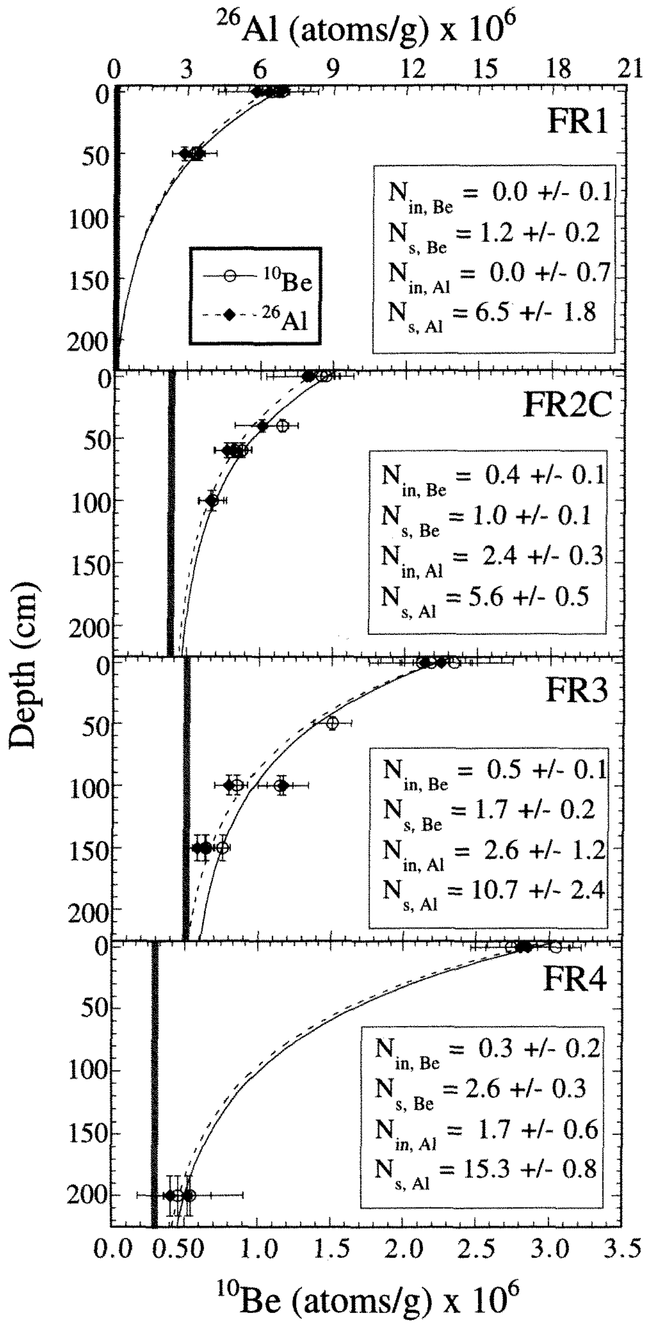

Figure 19. Plot of the full cosmogenic radionuclide concentration profiles for FR2C and FR3, and the amalgamated sample results used in the pairs techniques on all terraces. Note ^{26}Al (top axis) and ^{10}Be (bottom axis) are plotted on scales that differ by a factor of 6.0. Curves are fits to a shifted exponential with the length scale z fixed at 0.8 m (solid line ^{10}Be; dashed ^{26}Al). The fits yield similar values of inheritance for FR2C, FR3 and FR4. Inheritance on FR1 appears to be minimal.*

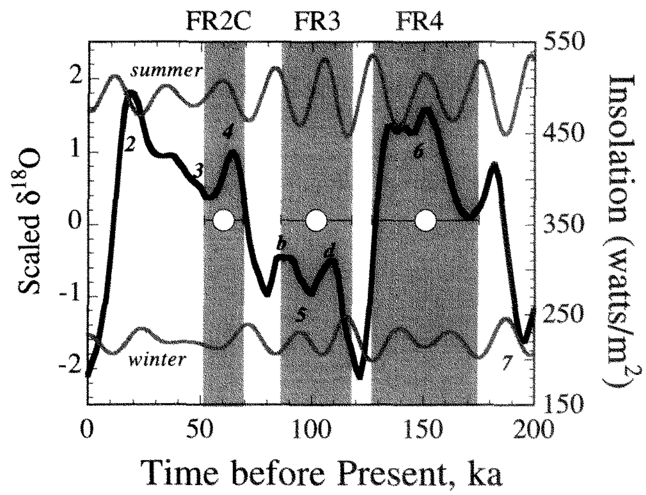

Figure 20. Age estimates of the three best dated terraces (FR2C, FR3, and FR4) shown against the last 250 ka of the normalized global δ^{18}O record (Imbrie et al., 1984); oxygen-isotope stages are numbered. The terrace ages (gray bars) were determined from production rates scaled to the Nishiizumi et al., (1996) calibrations, and post-depositional accumulations of cosmogenic radionuclides were constrained by fitting the concentration profiles shown in Figure 19. Also shown are the summer and winter insolation calculations of Berger and Loutre (1991) for 30°N. The terrace ages correspond roughly to global ice volume maxima in stages 4, 5d and 6, and to insolation histories of maxima in the summer and minima in the winter.

present in the area do not allow proper sampling with a sufficient degree of confidence in the results.

The terrace ages appear to support a glacial origin of the terrace gravels, and post-glacial abandonment of the surfaces. The previous assumption (Howard, 1986) that the largest two terraces correspond to the last glacial maximum and penultimate glaciations, by analogy with the Wind River sequence, must clearly be superseded by these absolute ages. That these small alpine systems apparently respond significantly to relatively minor global climate swings, as these results demonstrate for the Fremont, and as has been recently suggested for Sierran glacial systems (Phillips et al., 1996), makes regional correlations more difficult: One system is likely to respond more, or less, sensitively than another to the same fluctuations in regional climate.

COMBINED REFERENCES

Parts 1–5

Billingsley, G.H., Huntoon, P.W., and Breed, W.J., 1987, Geologic map of Capitol reef National Park and vicinity, Emery, Garfield, Millard and Wayne counties, Utah. Utah Geological and Mineral Survey, Map 87, 1.62.500.

Everitt, B.L., 1979, The cutting of Bull Creek arroyo: Utah Geology, v. 6, No. 1, p. 39–44.

Everitt, B.L, 1980, Vegetation and sediment migration in the Henry Mountains region, Utah, *in* Picard, 1980, p. 209–214.

Everitt, B.L., 1983, Preliminary foundation investigation, Blue Valley Dam site, Lower Fremont River. Utah Division of Water Resources report, 18 p.

Everitt, B.L , 1984, Potential for groundwater development in Caineville Utah Division of Water Resources memorandum, 4 p.

Everitt, B.L., 1987, Torrey dam site seismic refraction survey, lower Fremont project: Utah Division of Water Resources memorandum, 3 p.

Everitt, B.L., 1995a, Activity classification of the Thousand Lake Fault: Utah Division of Water Resources memorandum, 7 p.

Everitt, B.L., 1995b, Hydrologic factors in regeneration of Fremont Cottonwood along the Fremont River, Utah: Amer. Geophysical Union, Geophysical Monograph 89, p. 197–208.

Flint, R.F., and Denny, C.S., 1958, Quaternary geology of Boulder Mountain, Aquarius Plateau, Utah. U.S. Geological Survey Bulletin 1061-D, p. 103–164.

Gilbert, G.K., 1877, report on the geology of the Henry Mountains (Utah)· U.S. Geological and geographical Survey, Rocky Mountain Region (Powell), 160 p.

Godfrey, A.E , 1969, Geologic history and processes of fan and pediment development in the northern Henry Mountains piedmont, Utah: Ph.D. dissertation (unpublished), the John's Hopkins University, Baltimore, Maryland.

Godfrey, 1980, Debris avalanche deposits north of Mount Ellen Henry Mountains Symposium, Utah Geological Association Publication 8, M. Dane Picard, Editor, pp. 171–176.

Godfrey, 1997a, Wind erosion of Mancos Shale badland ridges by sudden drops in pressure: Earth Surface Processes and Landforms, v. 22, no. 4, p. 345–352.

Godfrey, 1997b, Mass movement of Mancos Shale crust near Caineville, Utah: a 30-year record: Geografiska Annaler, no 3.

Graf, W.L., 1983, Downstream changes in stream power in the Henry Mountains, Utah. Annals, Assoc Am. Geog. V. 73, No. 3, p. 373–387.

Hintze, L.F., 1988, Geologic history of Utah· Brigham Young University Geology Studies, Special Publication 7.

Howard, A.D., 1970, A study of processes and history in desert landforms near the Henry Mountains, Utah. Ph.D. dissertation (unpublished), The Johns Hopkins University, Baltimore, Maryland.

Howard, Alan D., 1994a, Badlands *in* Abrahams, A D., and Parsons, A.J., editors, Geomorphology of Desert Environments: Chapman and Hall, London, pp. 213–242.

Howard, Alan D , 1994b, A detachment-limited model of drainage basin evolution: Water Resources Research, V. 30, p. 2261–2285.

Hunt, C.B., Averitt, Paul, and Miller, R.L., 1953, Geology and geography of the Henry Mountains region, Utah. U.S. Geological Survey Professional Paper 228, 234 p.

Hunt, C.B., 1977, Around the Henry Mountains with Charlie Hanks: Utah Geology, Vol. 4, no. 2, p. 95–104.

Hunt, C.B., 1988, Geology of the Henry Mountains, Utah, as recorded in the notebooks of G.K Gilbert, 1875–76: Geol. Soc. Am Memoir 167, 229 p.

Laine, M.D , Anderson, P.B , and Caputo, M.V, 1991, Field Symposium road log section I: Price to Green River, *in* Chidsey, Thomas C., ed., 1991, Geology of east-central Utah. Utah Geol. Association, Publication 19, p. 347–362.

Mattox, S.R., 1991, Petrology, age, geochemistry, and correlation of the Tertiary volcanic rocks of the Awapa Plateau, Garfield, Piute, and Wayne Counties, Utah: Utah Geological Survey Misc. Publication 91-5, 46 p.

Midland Trail Association, 1916, Midland trail tour guide: Midland Trail Log Book Company, Grand Junction (facsimile reprint 1969, Rio Grande Press).

Oaks, Robert Q., 1988, Geology 350 fall field trip, Capitol Reef, Henry Mountains: Manuscript, Utah State University, 15 p.

Osterkamp, W.R., and Hupp, C.R., 1984, Geomorphic and vegetative characteristics along three northern Virginia streams. Geol Soc. Am. Bull., V. 95, p 1093–1101.

Palmer-Wilding, 1981, Preliminary design investigation, Caineville Dam, Lower Fremont River Report to Wayne County Water Conservancy District.

Picard, M.D., (ed.), 1970, Henry Mountains Symposium: Utah Geological Association Publication 8, 388 p.

Rich, J.L., 1935, Origin and evolution of rock fans and pediments. GSA Bull., v. 46, pp. 999–1024.

Rigby, J.K., 1976, Field Guide, Northern Colorado Plateau. Kendall/Hunt, 207 p

Schumm, Stanley A., and Gregory, Daniel I., 1986, Diffuse-source salinity· Mancos Shale Terrain: Bureau of Land Management Technical note 373

SHB AGRA, 1992, Engineering geology, geoseismic, and geotechnical study, proposed Torrey Dam and Reservoir. Report to Wayne County Water Conservancy District, SHB AGRA Job E90-2027.

Smith, J F., Jr., Huff, L.C , Hinrichs, E.N., and Luedke, R.G.,1963, Geology of the Capitol Reef area, Wayne and Garfield counties. U.S. Geological Survey Professional Paper 363, 102 p.

Van Cott, J.W., 1990, Utah Place Names: University of Utah Press, 453 p.

Webb, R.H., 1985, Late Holocene flooding on the Escalante River, South-central Utah PhD dissertation, University of Arizona, Tucson.

Wooley, Ralf R , 1946, Cloudburst floods in Utah, 1850–1938. U.S. Geol. Surv. Water Supply Paper 994, 128 p.

Part 6

Bryan, R.B., and Yair, A., 1982, Perspectives on studies of badland geomorphology, *in* Bryan, R.B., and Yair, A., eds., Badland geomorphology and piping: Norwich, Geo Books, p. 1–12.

Bryan, R.B., Imeson, A.C., and Campbell, I.A., 1984, Solute release and sediment entrainment on microcatchments in the Dinosaur Park badlands, Alberta, Canada· Journal of Hydrology, v 71, p. 79–106.

Bryan, R.B., Campbell, I.A., and Yair, A., 1987, Postglacial geomorphic development of the Dinosaur Provincial Park badlands, Alberta. Canadian Journal of Earth Sciences, v. 24, p. 135–146

Campbell, I.A., 1982, Surface morphology and rates of change during a ten-year period in the Alberta badlands, *in* Bryan, R.B., and Yair, A., eds., Badland geomorphology and piping· Norwich, Geo Books, p. 221–238.

Costa, J.E., and O'Connor, J.E., 1995, Geomorphically effective floods, *in* Costa, J.E., Miller, A.J., Potter, K.W, and Wilcock, P.R., eds., Natural and anthropogenic influences in fluvial geomorphology The Wolman volume. Geophysical Monograph 89· Washington, D C , American Geophysical Union, p. 45–56.

Dick, G.S , 1995, Documentation of flow in ephemeral channels, Upper Blue Hills, Utah [M.S. thesis]· Santa Cruz, University of California

Dick, G.S., Anderson, R.S., and Sampson, D.E., 1997, Controls on flash flood magnitude and hydrograph shape, Upper Blue Hills badlands, Utah Geology, v. 25, p. 45–48.

Hassan, M.A., 1990, Observations of desert flood bores: Earth Surface Processes and Landforms, v. 15, p. 481–485.

Howard, A.D., 1970, A study of process and history in desert landforms near the Henry Mountains, Utah [Ph.D. dissertation]. Baltimore, Johns Hopkins University.

Howard, A.D., 1994, Badlands, *in* Abrahams, A.D., and Parsons, A.J., eds., Geomorphology of Desert Environments: London, Chapman and Hall, p. 213–242.

Knighton, D., 1984, Fluvial forms and processes: London, Edward Arnold, 218 p.

Leopold, L.B., and Miller, J.P., 1956, Ephemeral streams—Hydraulic factors and their relation to the drainage net, U.S. Geological Survey Professional Paper 282-A, 37 p.

Lusby, G.C., 1979, Effects of grazing on runoff and sediment yield from desert rangeland at Badger Wash in western Colorado, 1953–1973, Volume 34, U.S. Geological Survey Water-Supply Paper 1532-I, 34 p.

Mesa, O.J., and Mifflin, E.R., 1986, On the relative role of hillslope and network geometry in hydrologic response, *in* Gupta, V.K., Rodriguez-Iturbe, I., and Wood, E.F., eds., Scale problems in hydrology: Dordrecht, Holland, D. Reidel, p. 1–17.

Reid, I., and Frostick, L.E., 1987, Flow dynamics and suspended sediment properties in arid zone flash floods: Hydrological Processes, v. 1, p. 239–253.

Renard, K.G., and Keppel, R.V., 1966, Hydrographs of ephemeral streams in the Southwest. American Society of Civil Engineers, Journal of the Hydraulics Division, v. 92, p. 33–52.

Schick, A.P., 1988, Hydrologic Aspects of Floods in Extreme Arid Environments, *in* Baker, V.R., Kochel, R.C., and Patton, P.C., eds., Flood Geomorphology: New York, Wiley-Interscience, p. 189–204.

Schumm, S.A., 1956, The role of creep and rainwash on the retreat of badland slopes: American Journal of Science, v. 254, p. 693–706.

Schumm, S.A., 1964, Seasonal variation of erosion rates and processes on hillslopes in western Colorado: Zeitschrift fur Geomorphologie Supplement Band 5, p. 215–238.

Schumm, S.A., and Lusby, G.C., 1963, Seasonal variation of infiltration capacity and runoff on hillslopes in western Colorado. Journal of Geophysical Research, v. 68, p. 3655–3666.

Yair, A., Lavee, H., Bryan, R.B., and Adar, E., 1980, Runoff and erosion processes and rates in the Zin Valley badlands, northern Negev, Israel: Earth Surf. Process., v. 5, p. 205–225.

Part 7

Anderson, R.S., Repka, J.L., and Dick, G.S., 1996, Explicit treatment of inheritance in dating depositional surfaces using *in situ* ^{10}Be and ^{26}Al: Geology, v. 24, p. 47–51.

Berger, A., and Loutre, M.F., 1991, Insolation values for the climate of the last 10 million of years: Quaternary Sciences Review, v. 10, p. 297–317.

Bierman, P., 1994, Using in situ produced cosmogenic isotopes to estimate rates of landscape evolution: A review from the geomorphic perspective: Journal of Geophysical Research-Solid Earth, v 99, p. 13,885–13,896.

Billingsly, G.H., Huntoon, P.W., and Breed, W.J., 1987, Geologic map of Capitol Reef National Park and vicinity, Emery, Garfield, Millard and Wayne Counties, Utah: Utah Geological and Mineral Survey, Salt Lake City, UT.

Bull, W.B., 1991, Geomorphic Responses to Climate Change. Oxford University Press, New York City, N.Y, 352 pp.

Cerling, T.E , and Craig, H., 1994, Geomorphology and in-situ cosmogenic isotopes: Reviews of Earth and Planetary Sciences, v. 22, p. 273–317.

Clark, D.H., Bierman, P.R., and Larsen, P., 1995, Improving *in situ* cosmogenic chronometers· Quaternary Research, v. 44, p. 367–377

Finkel, R.C., and Suter, M., 1993, AMS in the earth sciences. Technique and applications: Advances in Analytical Geochemistry, p. 1–114.

Flint, R.F., and Denny, C.S., 1956, Quaternary Geology of Boulder Mountain, Aquarius Plateau, Utah: U.S. Geological Survey Bulletin 1061-D, p. 103–164.

Howard, A.D., 1970, Study of process and history in desert landforms near the Henry Mountains, Utah. Ph.D. thesis, Johns Hopkins University, Baltimore, MD, 198 pp.

Howard, A.D., 1986, Quaternary landform evolution of the Dirty Devil River system, Utah: Geological Society of America Abstracts with Programs, v. 18, p. 641.

Imbrie, J., Hays, J.D., Martinson, D.G., McIntyre, A., Mix, A.C., Morley, J.J., Pisias, N.G., Prell, W.L., and Shackelton, N.J., 1984, The orbital theory of Pleistocene climate: support from a revised chronology of the marine δ^{18}O record, in· Milankovitch and Climate: Understanding the Response to Astronomical Forcing, Part 1, Berger, A., Imbrie, J., Hays, J., Kukla, G., and Saltzman, B., eds., Reidel Publishing, Higham, MA, p. 269–305.

Lal, D., 1991, Cosmic ray labeling of erosion surfaces: in situ nuclide production and erosion models. Earth and Planetary Science Letters, v. 104, p. 424–439.

Nishiizumi, K., Kohl, C.P., Arnold, J.R., Dorn, R.I., Klein, J., Fink, D , Middleton, R., and Lal, D., 1993, Role of in situ cosmogenic nuclides ^{10}Be and ^{26}Al in the study of diverse geomorphic processes: Earth Surface Processes, v. 18, p. 407–425.

Nishiizumi, K., Finkel, R.C., Klein, J., and Kohl, C.P., 1996, Cosmogenic production of ^{7}Be and ^{10}Be in water targets: Journal of Geophysical Research, v. 101, p. 22,225–22,232.

Phillips, F., Zreda, M.G., Benson, L.V., Plummer, M.A., Elmore, D., and Sharma, P., 1996, Chronology for fluctuations in late Pleistocene Sierra Nevada glaciers and lakes: Science, v. 274, p. 749–751.

Repka, J.L., Anderson, R.S., and Finkel, R.P., in press, Cosmogenic dating of fluvial terraces, Fremont River, Utah: Earth and Planetary Science Letters.

Wells, S.G., McFadden, L.D., Poths, J., and Olinger, C T., 1995, Cosmogenic ^{3}He surface-exposure dating of stone pavements—Implications for landscape evolution in deserts: Geology, v. 23, p. 613–617.

PART TWO

MESOZOIC TO RECENT GEOLOGY OF UTAH

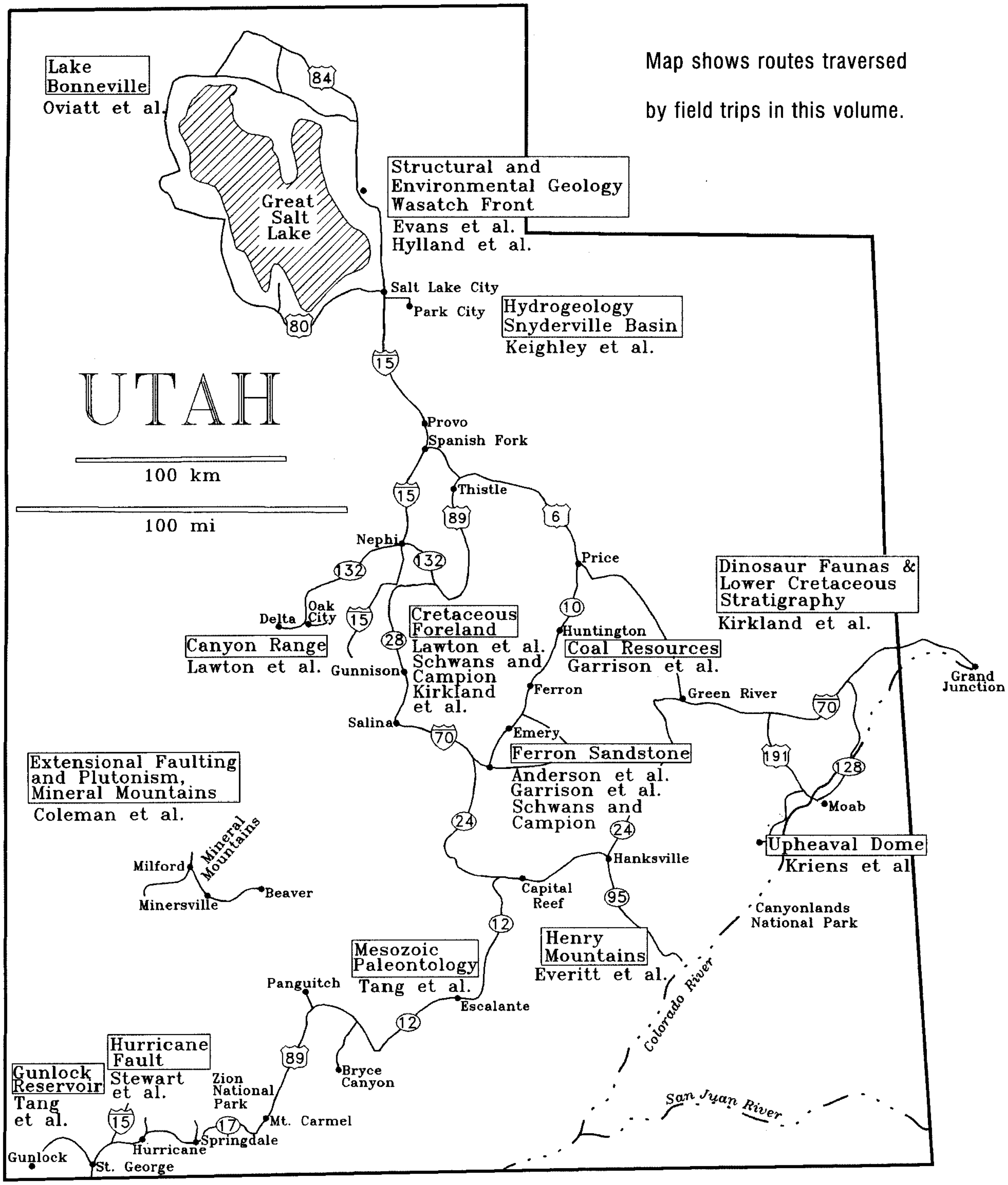

Map shows routes traversed by field trips in this volume.